Title: Therapeutic efficacy of antimalarial drugs targeting DosRS signaling in *Mycobacterium abscessus*

Authors: Juan Manuel Belardinelli[1], Deepshikha Verma[1], Wei Li[1], Charlotte Avanzi[1], Crystal J. Wiersma[1], John T. Williams[2], Benjamin K. Johnson[3], Matthew Zimmerman[4], Nicholas Whittel[1], Bhanupriya Angala[1], Han Wang[4], Victoria Jones[1], Véronique Dartois[4], Vinicius C. N. de Moura[1†], Mercedes Gonzalez-Juarrero[1], Camron Pearce[1], Alan R. Schenkel[5], Kenneth C. Malcolm[6,7], Jerry A. Nick[6,7], Susan A. Charman[8], Timothy N. C. Wells[9], Brendan K. Podell[1], Jonathan L. Vennerstrom[10], Diane J. Ordway[1], Robert B. Abramovitch[2], Mary Jackson[*1]

Affiliations:

[1]Mycobacteria Research Laboratories, Department of Microbiology, Immunology and Pathology, Colorado State University; Fort Collins, Colorado, USA.

[2]Department of Microbiology and Molecular Genetics, Michigan State University; East Lansing, Michigan, USA.

[3]Department of Epigenetics, Van Andel Institute, Grand Rapids, Michigan, USA.

[4]Center for Discovery and Innovation, Hackensack Meridian Health; Nutley, New Jersey, USA.

[5]Department of Microbiology, Immunology and Pathology, Colorado State University; Fort Collins, Colorado, USA.

[6]Department of Medicine, National Jewish Health; Denver, USA.

[7]Department of Medicine, University of Colorado; Anschutz Medical Campus, Aurora, Colorado, USA.

[8]Centre for Drug Candidate Optimisation, Monash Institute of Pharmaceutical Sciences, Monash University; Parkville, Victoria, Australia.

[9]Medicines for Malaria Venture; Geneva, Switzerland.

[10]College of Pharmacy, University of Nebraska Medical Center; Omaha, Nebraska, USA.

[*]Corresponding Author: Mary Jackson, Mary.Jackson@colostate.edu

[†]Present/Current Author Addresses: Vinicius Calado Nogueira de Moura; NTM Culture, Biorepository and Coordinating Core, National Jewish Health, Denver, Colorado, USA

One sentence summary: Repurposing of antimalarial drugs to treat pulmonary nontuberculous mycobacterial infections.

Abstract: A search for alternative *Mycobacterium abscessus* treatments led to our interest in the two-component regulator DosRS which, in *Mycobacterium tuberculosis*, is required for the bacterium to establish a state of non-replicating, drug-tolerant persistence in response to a variety of host stresses. We show here that the genetic disruption of *dosRS* impairs the adaptation of *M. abscessus* to hypoxia, resulting in decreased bacterial survival following oxygen depletion, reduced tolerance to a number of antibiotics *in vitro* and *in vivo*, and the inhibition of biofilm formation. We determined that three antimalarial drugs or drug candidates, artemisinin, OZ277, and OZ439, can target DosS-mediated hypoxic signaling in *M. abscessus* and recapitulate the phenotypic effects of genetically disrupting *dosS*. Importantly, OZ439 displayed bactericidal activity comparable to standard-of-care antibiotics in chronically infected mice, in addition to potentiating the activity of antibiotics used in combination. The identification of antimalarial drugs as potent inhibitors and adjunct inhibitors of *M. abscessus in vivo* offers repurposing opportunities that could have an immediate impact in the clinic.

Main Text:

INTRODUCTION

Rapidly-growing nontuberculous mycobacteria (NTM) of the *Mycobacterium abscessus* complex (MABSC; including *M. abscessus* subsp. *abscessus, M. abscessus* subsp. *massiliense* and *M. abscessus* subsp. *bolletii*), and slowly-growing NTM of the *Mycobacterium avium* complex (MAC) have emerged as important human pathogens globally, and are linked to an increasing number of pulmonary infections among patients with structural lung disease such as chronic obstructive pulmonary disease (COPD), bronchiectasis, and cystic fibrosis (CF) (*1-3*). The low cure rate of currently available treatment regimens, in spite of a minimum of 12 months of chemotherapy (in the range of 25–58% for MABSC pulmonary disease), notable side effects, and frequent bacterial re-emergence associated with these regimens highlight the need for alternative approaches to treat NTM infections (*4*). The radiographic appearance of MAC and MABSC pulmonary disease can be similar to tuberculosis (TB) and may include cavity formation, nodules, and airspace disease (*5-7*). When present, granulomas from MABSC-infected patients are histologically indistinguishable from lesions caused by *Mycobacterium tuberculosis* (*Mtb*) (*8*). The precise nature of the host stresses to which MABSC and MAC are exposed within these lesions and how the bacteria respond to them is not as well documented than for *Mtb*. Nevertheless, it is believed that NTM and *Mtb* share the ability to persist within the granulomatous structures in a non-replicating state, which contributes to their drug tolerance and to treatment failure in chronically-infected individuals (*4,8-10*). Further compounding this problem is the ability of MABSC and MAC to form what appears to be genetically programmed biofilms when in contact with human cells (*11-15*), and clinical evidence for MABSC biofilm formation within the thickened alveolar walls, airways, and lung cavity during pulmonary infections in patients with COPD or CF (*6,7,16*). Biofilm formation is a common strategy used by pathogens of the soft tissue

and airways to chronically infect the host and can enhance their drug tolerance and resistance to host defense mechanisms (*14,17-22*).

The inhibition of aerobic respiration caused by oxygen depletion or exposure to nitric oxide (NO) and carbon monoxide (*21,23-25*) is common stressor of intra- and extracellular pathogenic mycobacteria inside activated immune cells, in avascular necrotic regions of granulomas, and within microaggregates or biofilms. *Mtb* survives this stress *in vitro* and *in vivo* by inducing a regulon of 48 genes that drives its entry into a non-replicating state while adapting bacterial metabolism to maintain energy levels and a redox balance compatible with survival in the absence of respiration (*23,25-29*). This response is under control of the three-component regulatory system, DosRST, and inhibitors of the response regulator DosR and of the two sensor histidine kinases, DosS and DosT, are being sought for their potential to shorten tuberculosis treatment and lower relapse rates when used in combination with standard-of-care antibiotics (*30*).

MABSC species are endowed with a DosRS system, although they lack the sensor histidine kinase, DosT (*31*). The precise nature of the MABSC DosRS regulon has yet to be experimentally established, but a recent study identified the predicted DosR regulon genes of MABSC among genes whose expression was the most upregulated following exposure to NO-induced hypoxia (*31,32*). Further supporting a role for this two-component regulatory system (2CR) in the ability of MABSC to become a chronic pathogen of the lung, *dosR, dosS* and other predicted DosR-regulated genes were found to be expressed at higher levels in rough (R) than in smooth (S) morphotype variants of *M. abscessus* subsp. *abscessus* (*Mabs*) ATCC 19977 (*33*), the former variants being known for their hyperaggregative and hypervirulent phenotypes (*17,34*). In view of these findings, a detailed investigation of DosRS from MABSC was undertaken herein with the goal to define the contribution of this 2CR to MABSC drug tolerance and ability to survive under

microaerophilic conditions, including within biofilms. Genetic and chemical inhibition of DosRS *in vitro* and *in vivo* validate this regulator as a target of therapeutic interest whose inhibition has the potential to improve MABSC clearance and treatment outcomes.

RESULTS

DosRS from MABSC is required for persistence under hypoxia

To determine whether DosRS from MABSC responded to O_2 depletion, the level of expression of *dosR* and *dosS* in *Mabs* ATCC 19977 grown under well-aerated and microaerophilic conditions was compared by RT-qPCR. Twenty-four hours after exposure to microaerophilic conditions, when the level of expression of *dosR* and *dosS* peaked [Fig. S1], *dosR* expression was upregulated ~ 60-fold relative to cells grown under well-aerated conditions [Fig. 1A].

To assess the impact of disrupting the 2CR on the ability of MABSC to survive under hypoxia, we made a knock-out (KO) mutant of *Mabs* ATCC 19977 in which the entire *dosRS* operon was deleted by allelic replacement [Fig. S2]. Complemented mutants were generated by transforming the KO mutant, *Mabs*Δ*dosRS*, with integrative plasmids allowing for the expression of the entire *dosRS* operon or *dosR* only under control of their own promoter. Relative to the wild-type (WT) parental strain and mutant complemented with *dosRS*, *Mabs*Δ*dosRS* displayed a clear survival defect in the hypoxic Wayne model of non-replicating persistence (*35*) characterized by a greater than 1.2 to 1.4 $\log_{10}$ difference in CFUs after 21 d [Fig. 1B]. That this decrease in CFU counts reflected loss of viability rather than loss of culturability was verified by monitoring the fluorescence of similarly cultured mCherry-expressing bacterial strains over time. A similar proportion of mCherry-expressing WT, Δ*dosRS* and *dosRS* complemented KO bacilli were present

in the cultures at the onset of hypoxia, but the percentage of mCherry-expressing (i.e., viable) bacilli after 21 d of hypoxic growth was significantly less ($p < 0.005$) in the case of the mutant compared to the WT and *dosRS* complemented strains, indicative of the decreased viability of *Mabs*Δ*dosRS* [Fig. S3]. Importantly, *Mabs*Δ*dosRS* complemented with only the *dosR* gene did not survive better than the KO strain [Fig. 1B] indicating that the DosS sensor is required for MABSC to persist under these conditions.

Impact of DosRS on MABSC drug tolerance under hypoxia

DosRST has been shown to be required for *Mtb* tolerance to antibiotics during hypoxia, a phenotype in large part attributable to the upregulation of the DosR-regulated triglyceride synthase gene, *tgs1* (*36-38*). To assess the impact of DosRS on the drug tolerance of MABSC under non-replicating hypoxic persistence, *Mabs* ATCC 19977 WT, *Mabs*Δ*dosRS,* and *Mabs*Δ*dosRS* complemented with *dosRS* were grown in the same Wayne model as described above and, upon achieving hypoxia, treated for 7 d with antibiotics used in the clinical treatment of MABSC infections, including amikacin (AMK), azithromycin (AZI), imipenem (IMI), and clofazimine (CFZ) prior to enumerating surviving bacteria. The results indicated that while the WT and *dosRS* complemented mutant were fully tolerant to all antibiotics at the concentrations used herein, *Mabs*Δ*dosRS* displayed a significant ($p < 0.05$) 15, 64 and 52% decrease in survival compared to the DMSO-treated mutant control upon exposure to AMK, AZI and CFZ, respectively [Fig. 1C]. Lack of DosRS impaired the ability of MABSC to survive and establish a state of non-replicating, drug-tolerant persistence under hypoxia.

That the drug tolerance of MABSC resulted from the intracellular accumulation of triglycerides following O_2 depletion is unlikely given the result of a metabolic labeling experiment

that showed comparable [1,2-^{14}C]acetate incorporation into these lipids (and other major glycerolipid forms) in the mutant, WT, and *dosRS* complemented strains [Fig. S4]. This finding is in contrast to the situation in *Mtb*, but it is consistent with the different nature of the DosR regulon in the two species as will be described further.

Effect of DosRS inactivation on MABSC biofilm growth

Reasoning that the disruption of *dosRS* may impair MABSC response to redox stress and hypoxia and, thus, biofilm development, we sought to compare the WT and KO strains for their ability to form biofilms *in vitro*. The biofilm model used to perform this experiment, which was recently developed in our laboratory, uses a chemically-defined synthetic CF medium (SCFM) to grow MABSC as submerged biofilms in poly-D-lysine-coated plates (*39*). We have shown SCFM to closely mimic the nutritional conditions encountered and metabolic adaptation undergone by MABSC in actual CF sputum (*40*), making this model more relevant to infection than previously described models based on standard laboratory media (*4,41,42*).

The result from this experiment indicated that despite growing at a similar rate as the WT parent in SCFM under planktonic conditions [Fig. S5], the mutant was ~ 4-times less proficient at biofilm formation based on crystal violet staining [Fig. 2A]. This defect in biofilm formation also reflected in the number of CFUs associated with WT, mutant, and complemented mutant biofilms [Fig. 2B] and in the confocal fluorescence imaging, including thickness, of biofilms formed by mCherry-expressing WT and *dosRS* KO strains [Fig. 2]. Biofilm formation was largely restored in the *dosRS* complemented mutant but, again, not in the mutant complemented with *dosR* only [Fig. 2A, 2B, 2E].

Effect of disrupting dosRS on the susceptibility of MABSC to antibiotics in vivo

The impact of disrupting *dosRS* on *Mtb* pathogenesis has proven to be dependent on the animal model used, primarily because DosRS-related phenotypes only clearly express in organized hypoxic lesions (*30*). C3HeB/FeJ mice provide such an environment (*26*), but their natural resistance to MABSC infection unless continuously treated with corticosteroids limited their potential for the proposed studies (*43,44*). The effect of disrupting *dosRS* on the virulence and persistence of MABSC *in vivo* was thus determined in SCID mice due to their permissiveness to MABSC infection and the human-like non-necrotizing and necrotizing granulomas as well as large numbers of foamy cells they develop in which non-replicating MABSC may reside (*44*). The WT and mutant strains replicated and persisted similarly in the lungs and spleen of these mice over the course of 56 d [Fig. 3]. However, when treated with AMK upon establishment of chronic infection (i.e., as of d 28), significantly ($p < 0.05$) greater bacterial clearance was observed in the case of the mutant compared to the WT parent strain in both organs [Fig. 3]. Restoration of WT-like growth in mice infected with the *dosRS* complemented mutant was visible in the spleen, where the greatest difference between WT and mutant strains was noted, but not in the lungs of AMK-treated animals. The reason for the successful *dosRS* complementation of the knock-out mutant in all *in vitro* assays and in the spleen of AMK-treated animals but not in the lung is at present unclear but could be due to apparent differences in the level of expression of *dosRS* in the complemented strain compared to the WT parent [Fig. S1].

Collectively, our results supported DosRS as a target of therapeutic interest in MABSC for the potential of inhibitors of this 2CR to impair the ability of MABSC to survive under hypoxic conditions, develop a drug-tolerant persistent state, and form biofilms.

Disruption of MABSC biofilm formation, persistence and drug tolerance under hypoxia by inhibitors of the DosS sensor kinase

A number of inhibitors have been reported to target DosRST signaling in *Mtb*, including the antimalarial drug artemisinin (ART) and analogs (artesunate [AS], artemether, and dihydroartemisinin), and HC106A (1-(2,4-dichlorophenyl-3-(1,2-oxazol-5-yl)urea) (*29,30,45*) [Fig. 4A]. Given the conservation of the DosS proteins from *Mtb* and MABSC (52% amino acid identity, 68% similarity on a 572 amino acid overlap), we sought to determine whether *Mtb* DosS inhibitors were capable of recapitulating in MABSC any of the phenotypic effects associated with the genetic disruption of *dosRS*. The compounds used in these studies included the optimized HC106A analog, MSU-39446, ART, AS and two synthetic peroxides chosen for their much-improved pharmacokinetic (PK) properties over ART and AS: OZ277 (arterolane; a registered antimalarial drug) and OZ439 (artefenomel; currently in phase 2 clinical trial for the treatment of malaria) (*46-50*) [Fig. 4A]. All compounds displayed Minimum Inhibitory Concentrations (MICs) against *Mabs* ATCC 19977 in SCFM and cation-adjusted Mueller-Hinton II media equal to (OZ439) or greater than (all other compounds) 400 μM. Higher concentrations were not tested due to solubility issues.

The effect of ART and OZ439 on the ability of MABSC to persist under hypoxia was first determined by adding 40 μM of each compound to hypoxic cultures of *Mabs* ATCC 19977 and enumerating surviving bacteria after 7 d of incubation [Fig. 4B]. Compared to the DMSO-treated controls, the WT and *dosRS* complemented strains suffered a significant ($p < 0.005$) decrease in viability upon exposure to either of the compounds (1.12 and 0.64 $\log_{10}$ CFU for ART; 1.18 and 0.72 $\log_{10}$ CFU for OZ439, respectively). *Mabs*Δ*dosRS*-treated cells, in contrast, did not exhibit

any significant decrease in viability (beyond that caused by 7 d of hypoxic growth) compared to the DMSO control, indicative of the on-target activity of the compounds.

Pretreatment of hypoxic WT *Mabs* ATCC 19977 cultures with either DMSO, ART or OZ439 for 3 d prior to incubation with AMK, AZI or CFZ for another 7 d further caused a significant ($p < 0.05$) decrease in the tolerance of the ART- and OZ439-treated cells to AZI, and a decrease in the tolerance of the ART-treated cells to AMK, whereas tolerance to CFZ was unaffected by DosS inhibitor treatment [Fig. 4C]. In line with the absence of DosS sensor in the *dosRS* knockout mutant, DosS inhibitor treatment did not significantly enhance the susceptibility of the mutant to AMI or AZI [Fig. S6].

Finally, when tested in our biofilm assay, ART, AS, OZ277, and OZ439 all inhibited biofilm formation with IC_{50} values (required to inhibit 50% of biofilm formation) of 0.8 - 1.6 μM [Fig. 5A-B]. MSU-39446 was the least active with an IC_{50} value of ~ 50 μM. When added to established 4-d old *Mabs* ATCC 19977 biofilms, none of the compounds dispersed the biofilms under the conditions of our assay, indicating that they were most active in preventing biofilm formation [Fig. S7].

Inhibition of DosRS signaling by artemisinin and synthetic peroxides

To investigate the inhibitory mechanism of ART and OZ439, RNA sequencing-based transcriptional profiling was undertaken on *Mabs* ATCC 19977 treated with 20 μM of the inhibitors or DMSO as a control under microaerophilic conditions, and the results were compared to the transcriptional profiles of similarly treated *Mabs*Δ*dosRS* cells.

Since the DosR regulon genes of MABSC had not been experimentally characterized, a detailed comparison of the transcriptional profiles of WT *Mabs* ATCC 19977 and the *dosRS* KO

mutant in the absence of inhibitor treatment was conducted. The list of differentially expressed (DE) genes ($\log_2$ fold change > 2 with a false discovery rate adjusted p-value < 0.05) was compared to the known DosR regulon of *Mtb* (*25,28*) and the bioinformatically-predicted DosR regulon from MABSC (*31*). A total of 38 genes were found to be differentially expressed, 21 of which fall within 7 gene clusters [Fig. 6A; Tables S1 and S2]. As in other mycobacteria, the DosR regulon of MABSC contains regulators, two universal stress proteins, and a number of genes involved in the maintenance of energy levels and redox potential in the absence of aerobic respiration (*31,51*). The latter include a nitroreductase (MAB_3903) and a nitrate ABC transporter, allowing for the use of nitrate as terminal electron acceptor, a ferredoxin (MAB_2240), the cytochrome c oxidase constituent CtaD (MAB_1042c), the succinate dehydrogenase MAB_2244, and oxidoreductases [Table S1]. Interestingly, the polyphosphate kinase gene *ppk2* (*MAB_1040*) was among the genes expressed at significantly ($p < 0.05$) lower level in the *dosRS* mutant compared to the WT strain. In *Mtb*, Ppk2 hydrolyzes polyphosphate, and the accumulation of this important signaling molecule in a *ppk2* mutant was shown to impair the ability of *Mtb* to form biofilms (*52*). Among DE genes are *MAB_2489* and *MAB_3902c,* which both have been proposed to be involved in aminoglycoside resistance (*53,54*) and might contribute to the observed hyper-susceptibility of *MabsΔdosRS* to this class of antibiotics *in vitro* and *in vivo* [Fig. 6A, Fig. 1C and Fig. 3]. Finally, at least three other genes (*MAB_0894c* encoding a lipoamide dehydrogenase; *MAB_3134c* encoding a transcriptional regulator and NO sensor, and *MAB_2530c* encoding a catalase) are expected to contribute to the intracellular survival of MABSC by protecting the bacilli from host-reactive nitrogen intermediates and reactive oxygen species (*40,55*). A consensus motif was identifiable in the promoter regions of ten of the DE genes or gene clusters of MABSC, which likely represents the binding site of DosR [Fig. S8]. Other DE genes that do not appear to be part

of the DosR regulon are likely the result of weak binding by DosR or indirect consequences of the inability of MABSC to activate the DosR regulon under microaerophilic conditions.

DE genes that changed upon treatment of WT *Mabs* with ART and OZ439 (log_2 fold change > 1 with a false discovery rate adjusted *p*-value < 0.05) showed a striking overlap with the list of DE genes between WT and *dosRS* KO (log_2 fold change > 2 with a false discovery rate adjusted *p*-value < 0.05), even though the magnitude of the changes in expression was less in the inhibitor-treated cells compared to the KO in which DosRS activity is completely abolished [Fig. 6B; Tables S1 and S2]. ART treatment repressed the expression of half of the genes that are also downregulated in the *dosRS* KO, whereas OZ439 had a milder effect inhibiting five common genes at the cut-off values set herein. These changes in gene expression indicate that both ART and OZ439 have the ability to prevent the induction of the DosRS regulon under microaerophilic conditions. RT-qPCR confirmed the RNA-seq data for five DosR regulon genes [Fig. S9].

Changes in gene expression in the KO mutant upon exposure to ART and OZ439 were analyzed and compared to the effects of treating the WT strain, with the premise that inhibitors specifically targeting the DosS protein of MABSC will not modulate gene expression in *Mabs*Δ*dosRS*, The mutant treated with ART and OZ439 exhibited only 22 and 10 downregulated genes, respectively, confirming the relative on-target specificity of these compounds [Table S2].

Since the DosRS pathway of MABSC has been reported to be induced by NO (*32*), we used RT-qPCR to determine whether ART, OZ439, and MSU-39446 inhibited the induction of DosR-regulated genes in WT *Mabs* ATCC 19977 following treatment with spermine/nitric oxide (Spermine/NO) for 40 min. Whereas the expression of *dosR* was induced by more than 240-fold in response to NO, none of the inhibitors tested inhibited NO-signaling [Fig. S10].

Artemisinin, synthetic peroxides, and MSU-39446 target the sensor kinase heme of MABSC DosS

A UV-visible spectroscopy assay was employed to verify that ART, OZ439, and MSU-39446 inhibited MABSC DosS through modulation of its redox status. To this end, the DosS protein from MABSC was expressed and purified from *E. coli* as described under Materials and Methods. DosS purified under aerobic conditions has a Soret peak at 410 nm [Fig. 7]. Reduction of the heme by dithionite (DTN) shifts the DosS Soret peak to 427 nm. The addition of ART to the reaction mixture caused the Soret peak of DosS to gradually shift back towards the oxidized Soret peak (421 nm at time 0, 414 to 412 nm after 30 or 60 min of incubation). A similar shift towards the oxidized position was also visible upon treatment of purified DosS with OZ439 and MSU-39446. As expected, degassed DMSO did not shift the peak whereas aerated DMSO fully shifted the peak back to the oxidized position [Fig. 7].

Adjunct therapeutic potential of DosS inhibitors in acute and chronic murine models of MABSC infection

Given the ability of DosS inhibitors to decrease the biofilm-forming capacity as well as the survival and drug tolerance of MABSC under hypoxic or microaerophilic conditions, we assessed the therapeutic potential of OZ439 and OZ277 in an *in vivo* model of MABSC infection, when used alone and in combination with antibiotics. These experiments used similar SCID mouse models as used to compare the virulence and drug tolerance of the WT and *dosRS* KO mutant [Fig. 3]. OZ277 and OZ439 were selected as test compounds for these studies for their safety profile and much improved PK properties over ART.

An acute model of MABSC infection was used in an initial experiment in which mice were infected intratracheally with $1.0x10^6$ CFUs of WT *Mabs* ATCC 19977. On d 12 post-infection during the acute phase of infection (*44*), mice were treated daily (7 d a week; every other day for OZ439 owing to the very long half-life of this compound) for 14 days with vehicle used in the formulation of OZ277 and OZ439 (HPMC-SV; see Materials and Methods), OZ439 (200 mg/kg, gavage), OZ277 (200 mg/kg, gavage), AMK (150 mg/kg, subcutaneous injection), AZI (200 mg/kg, gavage), IMI (100 mg/kg, subcutaneous injection), CFZ (20 mg/kg, gavage), and the same four antibiotic treatments in combination with OZ277 or OZ439. Groups of mice were ethically euthanized on d 2, 12 and 26, and processed for bacterial loads in the lungs, liver and spleen. In addition, four MABSC-infected mice that received OZ277 and OZ439 alone by gavage were ethically euthanized on d 26 for comparison of drug concentrations in the plasma and lung tissues at 2, 24, or 48 h after the last dosing. The results indicated good exposure for both compounds with concentrations in the lungs 2, 24, or 48 h after the last oral dosing [Fig. 8A and S11A] (~ 55 to 120 μM for OZ439; ~ 10 to 37 μM for OZ277), well above those needed to inhibit biofilm formation in our SCFM model [Fig. 5A]. OZ277 and OZ439 by themselves significantly reduced bacterial burdens in all organs of infected mice ($p < 0.05$), with the exception of OZ439 in the spleen [Fig. 8B and Fig. S11B]. Remarkably, the reduction in bacterial load in the lung following OZ439 treatment for 14 d (~ 1.8 $\log_{10}$) was of similar magnitude as that observed upon treatment with CFZ and IMI [Fig. 8B]. When used in combination with antibiotics, OZ439 further potentiated the activity of AZI, IMI and CFZ in the spleen and/or lung, resulting in significantly ($p < 0.05$) greater reduction in bacterial loads in these organs than seen in infected animals treated with antibiotics alone [Fig. 8B].

In a follow-up experiment, the therapeutic efficacy of OZ439 at the reduced dose of 50 mg/kg, alone or in combination with the same four antibiotics, was tested in a chronic SCID mouse model of MABSC infection. Mice were infected intravenously with $1.0x10^6$ CFUs of WT *Mabs* ATCC 19977. On d 28 post-infection, upon establishment of chronic infection (*44*), mice were treated daily (7 ds a week; every other day for OZ439) for 28 d with formulation vehicle, OZ439 (50 mg/kg, gavage), AMK, AZI, IMI and CFZ (same dosing as in the previous experiment) and the same four antibiotics in combination with OZ439. Determination of OZ439 exposure in this model indicated concentrations in the lungs 2 and 48 h after the last oral dose in the range of 6.2 and 3.9 μM, respectively, still above those needed to inhibit biofilm formation in SCFM and considerably below the MIC value of OZ439 in laboratory medium (400 μM) [Fig. 8A]. Analysis of bacterial loads in the lungs, liver, and spleen of the different treatment groups on d 2, 28 and 56 indicated that the efficacy of OZ439 by itself was comparable to that of all four antibiotics in the chronic model suggestive of the greater activity of the DosS inhibitor during the chronic vs. acute phase of infection [Fig. 8B and 8C]. When used in combination with antibiotics, OZ439 potentiated the activity of AZI in the liver and that of AMK in the lung and liver.

DISCUSSION

The existence of different microenvironments within the host is likely to drive intra- and extracellular NTM into distinct physiological states and may explain why NTM infections are usually incurable with antibiotic therapy alone and why adjunctive surgical resection of infected tissues may improve cure. MABSC bacilli located inside activated macrophages, in avascular necrotic granulomas, and within biofilms are exposed to O_2 depletion and NO-induced hypoxia.

Here, we show that a critical element of the adaptation of MABSC to these stresses is the two-component regulatory system DosRS. Unlike the situation in *Mtb* in which DosS is not critical to the activation of the DosR regulon, most likely as a result of the existence of a compensatory sensor kinase (DosT) (*26*), a functional DosS is essential to the induction of DosR upon O_2 depletion in MABSC. In line with this observation, inhibitors targeting the sensor heme of MABSC DosS phenocopy the effects of genetically disrupting *dosRS* or *dosS* in terms of inhibition of biofilm formation and decreased survival and drug tolerance under hypoxia.

RNA-seq analysis of the MABSC DosR regulon provides insights into the metabolic adaptation driving the ability of the bacilli to maintain energy levels and a redox balance in the absence of respiration. Other differentially expressed genes of interest between the WT and *dosRS* KO mutant include genes expected to promote intracellular survival by protecting MABSC from host-reactive nitrogen intermediates and reactive oxygen species (*MAB_0894c*, *MAB_3134c*, *MAB_2530c*), a DosRS regulon gene controlling polyphosphate concentrations in the cells (*MAB_1040*), which is likely to play a role in biofilm development (*52*), and two *Mtb*-conserved genes proposed to be involved in aminoglycoside resistance (*MAB_3902c* and *MAB_2489*) that may account for the potentiation of the activity of AMK against the *dosRS* mutant and DosS inhibitor-treated WT bacilli *in vitro* and *in vivo* [Fig. 1, 4 and 8].

A limitation of our study is the inability of SCID mice to faithfully model the lung pathology associated with MABSC infections in humans, in particular the development of hypoxic lesions (*44*), which may have led to an underestimation of the importance of DosRS in the pathogenicity of MABSC. However, the chronic SCID mouse model still pointed to the hyper-susceptibility of the *dosRS* null mutant to AMK and, to a lesser extent, AZI *in vivo* [Fig. 3]. In this regard, OZ439 treatment phenocopied the effect of genetically disrupting *dosRS* in that co-treating

MABSC-infected mice with this compound and either AZI or AMK tended to potentiate the activity of these antibiotics [Fig. 8].

A rather unexpected finding of this study was the dramatic reduction in MABSC loads following treatment with OZ439 by itself, and to a lesser extent OZ277, in both acutely and chronically infected mice. OZ439 when given orally at 200 mg/kg displayed an efficacy comparable to that of CFZ and IMI in the first model, and its efficacy was comparable to that of all four antibiotics tested herein (AMK, AZI, CFZ and IMI) in the chronic model despite reduced dosing (50 mg/kg). These results suggest that OZ439 is most active during the chronic phase of infection. The weaker activity of OZ277 compared to OZ439 is likely explained by the less favorable PK properties of the former.

Multiple factors may explain the dramatic decrease in survival of DosS inhibitor-treated WT *Mabs in vivo* whereas the *dosRS* KO mutant failed to show any virulence attenuation in the same mouse model. One important difference between the two studies resides in the differential effects of infecting mice with an MABSC strain devoid of DosR and DosS proteins from the onset of infection, and an MABSC strain that produces both proteins but whose DosS activity is pharmacologically and thus only partially inactivated once the infection is established. In *Mtb*, the production of DosR-regulated antigens (which would be expressed in a WT strain before the initiation of OZ439 treatment but not in a *dosRS* deletion mutant) has been implicated in the magnitude and timing of adaptive immune responses (*56,57*). DosS from *Mtb* has further been associated with DosR-independent activities such as the phosphorylation of a subset of proteins that may also impact the course of infection (*58*). Dissimilarities in antigen repertoires and bacterial adaptations to the host couldaccount for differences in the susceptibility of the *dosRS* KO and DosS inhibitor-treated WT bacilli to immune clearance, including in SCID mice that lack the

ability to mount normal adaptive immune responses. In spite of the relative specificity of ART and OZ439 for DosS at the concentrations used in the RNA-seq analysis, one cannot exclude the possibility that these compounds further display off-target bactericidal activity *in vivo*, especially at the relatively high concentrations achieved by OZ439 in the lungs of infected SCID mice. Alternatively, the activity of OZ439 and OZ277 could be host-directed. Indeed, an intriguing property of artemisinins is their ability to enhance autophagy and lysosomal killing (*59,60*). Determining whether OZ277 and OZ439 share this activity with ART and to what extent this activity might contribute to the intracellular killing of MABSC would be of great interest in further deciphering the therapeutic properties of these compounds.

A critical finding of this study is the identification of orally available antimalarial drugs and drug candidate with the potential to improve MABSC treatment both as a stand-alone therapy and when used by in combination with standard-of-care antibiotics. The repurposing of these agents provides a much-needed opportunity for innovative combination chemotherapy that could be available in the foreseeable future for patients suffering from MABSC infections.

MATERIALS AND METHODS

Study Design

The objectives of this study were to assess the therapeutic potential of the DosRS two-component regulatory system of MABSC and to identify potent inhibitors of this regulator active *in vivo*. A *dosRS* KO mutant of *Mabs* ATCC 19977 was constructed. and this mutant was compared to its WT parental and complemented mutant strains for its ability to survive and develop drug tolerance

under hypoxia, and form biofilms. The same KO mutant was compared to the WT parental strain for virulence and drug tolerance in a chronic SCID mouse model of MABSC infection. Subsequently, compounds known to inhibit DosS hypoxic signaling in *Mtb* and derivatives of these compounds with improved PK properties were tested for their ability to phenocopy the effect of genetically disrupting *dosRS in vitro*. Gene transcriptional profiling experiments and biochemical assays with compounds displaying activity *in vitro* confirmed that they abolish DosS signaling in MABSC. Finally, two of the compounds were evaluated for therapeutic and adjunct therapeutic efficacy in acute and/or chronic mouse models of MABSC infection. All protocols were approved by the Colorado State University institutional biosafety committee. All *in vitro* experiments were repeated at least two times. All *in vivo* procedures were reviewed and approved by the Colorado State University Animal Care and Usage Committee.

Strains and culture media

Mabs ATCC 19977 WT (smooth morphotype) and recombinant strains were grown under agitation at 37°C in Middlebrook 7H9 medium supplemented with 10% albumin-dextrose-catalase (ADC) (BD Sciences) and 0.05% Tween 80, in cation-adjusted Mueller Hinton II broth (BD Sciences) with 0.05% tyloxapol, in SCFM, or on Middlebrook 7H11 agar supplemented with 10% oleic acid-albumin-dextrose-catalase (OADC) (BD Sciences). Zeocin (Zeo) and kanamycin (Kan) were added to the culture media at a final concentration of 100 mg mL^{-1} and 200 mg mL^{-1}, respectively. For growth under microaerophilic and hypoxic conditions, *Mabs* was grown in Dubos-Tween albumin broth at a final pH of 7.25 either in standing T25 vented tissue culture flasks (microaerophilic conditions) (*45*) or in 16x100 mm glass tubes with tightly sealed screw caps with rubber septa under constant stirring using Teflon-coated magnetic bars (hypoxic Wayne model)

(*35*). Decolorization of methylene blue (1.5 mg mL^{-1} final concentration) in control tubes served as a visual indication of oxygen depletion in the Wayne model.

Mabs dosRS knock-out mutant and complemented mutant strains

A variation of the *katG*-based counterselection method described by Sander and collaborator (*61*) was used to generate a *dosRS* deletion mutant of *Mabs* ATCC 19977. The expression of the *katG* gene from *Mtb* in MABSC renders this species susceptible to isoniazid. Briefly, an allelic exchange substrate consisting of the zeocin-resistance cassette (*zeo*) and the colored marker *xylE* bracketed by ~ 1,000 bp of upstream and downstream DNA immediately flanking the *dosRS* operon of *Mabs* ATCC 19977 (*MAB_3891c-MAB_3890c*) was cloned in pKATs, a derivative of the replicative *E. coli – Mycobacterium* shuttle plasmid pMP349, harboring the *Mtb katG* gene (*61*). The resulting plasmid, pKATs-*dosRS::zeo-xylE*, was electrotransformed in *Mabs* ATCC 19977 and a transformant selected on zeocin-containing agar plates. Upon a culturing step in liquid broth, the transformant was finally plated on agar with zeocin and 512 mg mL^{-1} of isoniazid to select for allelic exchange mutants. Allelic replacement at the *dosRS* locus was verified by PCR and sequencing. For complementation, 220-bp of the promoter region of *dosR* and the entire coding sequence of *dosRS* were PCR-amplified from *Mabs* ATCC 19977 genomic DNA and cloned into the integrative plasmid pMV306, yielding pMV306-*dosRS.* Alternatively, 220-bp of the promoter region of *dosR* and the entire coding sequence of the only *dosR* gene were PCR-amplified and cloned into the integrative plasmid pMV306, yielding pMV306-*dosR.* The sequences of the primers used to generate the different constructs are available upon request.

MIC determinations and drug tolerance assays

The MIC values of DosS inhibitors were determined in cation-adjusted Mueller-Hinton II broth and in Synthetic Cystic Fibrosis Medium (*62*) devoid of mucin and DNA (herein referred to as SCFM), in a total volume of 200 µl in 96-well microtiter plates. *Mabs* cultures grown to early log phase were diluted to a final concentration of 10^5 CFU mL^{-1} and incubated in the presence of serial dilutions of the drugs for 5 d at 37ºC. MICs were determined using the resazurin blue test (*63*). Drug tolerance assays under hypoxia were conducted in the Wayne model of non-replicating persistence. Cultures of WT *Mabs* ATCC 19977, the *dosRS* KO and the complemented mutant strains grown in Dubos-Tween albumin broth to hypoxia (as determined by the decolorization of methylene blue) were added antibiotics and further incubated for 7 d prior to enumeration of surviving bacteria by CFU plating. When DosS inhibitors were used, *Mabs* cultures were grown to hypoxia as above in the presence of 40 µM of the DosS inhibitors from the time of inoculation; as cultures reached hypoxia, antibiotics and more DosS inhibitors (40 µM) were added and the cultures were left to incubate for 7 d prior to CFU plating.

Biofilm assays

MABSC submerged biofilms were formed in 96-well (polystyrene, flat bottom) poly-D-lysine-coated plates in SCFM medium, in the presence or absence of DosS inhibitors. Biofilm formation was monitored by crystal violet staining as follows: Culture medium and planktonic cells were removed from 5-d-old biofilm plate and biofilms were washed gently with PBS prior to adding 100 µL of 0.05% crystal violet solution. After 30 min of incubation at room temperature, the wells were washed with PBS and crystal violet was extracted with 300 µL of 30% acetic acid for 30 min followed by the reading of the absorbance of the solution at 600 nm. The absorbance resulting

from the binding of crystal violet to the poly-D-lysine coating was subtracted from all values reported on the graphs presented in Fig. 2A, Fig. 5A and Fig. S7.

For fluorescence confocal imaging, WT *Mabs* ATCC 19977, the *dosRS* KO and the *dosRS* complemented mutant strains were transformed with pCHERRY3 (Addgene # 24659) expressing mCherry. MABSC biofilms were grown for 2 to 6 d on poly-D-lysine-coated µ-Dish $^{35mm, low}$ (ibidi) at 37°C in a 5% CO_2 incubator. Biofilms were visualized using a KEYENCE BZ-X700 fluorescence microscope or a ZEISS LSM 510M ETA confocal microscope equipped with a 63x/1.40 plan-Apochromat objective. Two to three independent experiments were performed. Eight to ten different fields were analyzed per strain or treatment condition and images from one representative experiment/field are shown.

Whole cell radiolabeling

Metabolic labeling of *Mabs* cells with [1,2-^{14}C]acetic acid (0.5 µCi mL^{-1}; specific activity, 54.3 Ci/mol, PerkinElmer) was performed for 24 hs at 37˚C in Dubos-Tween albumin broth under microaerophilic conditions in standing T25 vented flasks. [1,2-^{14}C]acetic acid-derived lipids extracted from whole bacterial cells with a mixture of chloroform and methanol (1:2 and 2:1, by vol.) were analyzed by thin-layer chromatograph (TLC) on aluminum-backed silica gel 60-precoated plates F254 (E. Merck) and revealed by PhosphorImaging.

RNA extraction, reverse transcription and RT-qPCR

Two independent cultures of untreated and inhibitor-treated bacteria grown under microaerophilic conditions in Dubos-Tween albumin broth were used for transcriptomics analyses. RNA extraction with the Direct-zol™ RNA Miniprep kit (Zymo Research), reverse transcription reactions using

the Superscript IV First-Strand Synthesis System (Thermo Fisher) and RT-qPCRs using the SYBR Green PCR Master Mix (Sigma-Aldrich) were conducted as per the manufacturers' protocols and analyzed on a CFX96 real-time PCR machine (Biorad). PCR conditions: 98°C (30 s; enzyme activation), followed by 40 cycles of 98°C (10 s; denaturation) and 60°C (30 s; annealing/extension). Mock reactions (no reverse transcription) were done on each RNA sample to rule out DNA contamination. The target cDNA was normalized internally to the *sigA* cDNA levels in the same sample. The following primers were used: MAB_1042c_Fw (5'- ATCGGACTGGAGGCGGATCG -3') , MAB_1042c_Rv (5'- AAGAATGGTAGGGCCAGCAC -3'); MAB_2489_Fw (5'- CGTCCTTGTCGAGCTATCCA -3'), MAB_2489_Rv (5'- CTGCCATCATCCCGGTAAAC -3'); MAB_3354_Fw (5' CCGACCTCGAGCTCCTACAC -3'), MAB_3354_Rv (5'- GGATGTAGTCGTGCGGGTTCC -3'); MAB_3902c_Fw (5'- GCTCACTACGGTCGACCTTA -3'), MAB_3902c_Rv (5'- AGGCCATCCCTCCGACCAAA -3'); MAB_3903_Fw (5'- CAGACCGCTATCCAACTTGC -3'), MAB_3903_Rv (5'- GGTCCAGATACAGGTGCAGA -3'), and *sigA*_fwd (5'- CGTTCCTGGACCTGATTCAG -3'), *sigA_rev* (5'- GTACGTCGAGAACTTGTAACCC -3').

RNA-seq library preparation

RNA was quantified using a Qubit RNA spectrophotometer (Thermo Fisher) and sample quality was assessed using an Agilent High Sensitive RNA Screentape on an Agilent Tapestation, according to the manufacturer's recommendations. All RNA had an RNA Integrity Number (RIN) of greater than 6, indicating sufficient RNA quality for sequencing. Ribosomal RNA depletion was performed using an adapted protocol from Huang *et al*. (*64*). ssDNA oligo probes were designed to cover *Mabs* 16s and 23s rRNA using the RNaseH_depletion scripts

(https://github.com/hym0405/RNaseH_depletion) developed by Huang *et al.* (*64*) The ssDNA oligo probe sequences are available in Table S3. The oligo probe library was chemically synthesized (Integrated DNA Technologies Inc.), resuspended in a plate format (100 µM), and equimolarly pooled to generate the oligo probe mix used in this study. Ribosomal RNA was depleted from 0.5 µg of total RNA using a 5X probe ratio and 3 µL Hybridase Thermostable RNase H (Lucigen) as recommended by Huang *et al.* (*64*). Probes were then removed by DNAse treatment (Thermofisher) followed by a 2X bead clean-up (AMPure RNA, Beckman Counter). Depleted RNA was resuspended in the fragmentation buffer provided with the KAPA RNA Hyperprep kit (Roche). Fragmentation was performed for 6 min at 85°C followed by the 1st and 2nd strand synthesis. Ligation was performed with 1.5 µM of Kapa Dual-Indexed Adapter (Roche). After the final amplification step (5 cycles), libraries were quantified using Qubit dsDNA BR Assay Kit (Thermo Fisher Sc., USA, MA), and the fragment size was assessed on an Agilent Tapestation using the D1000 Screen tape. Libraries were multiplexed on one sequencing run at equimolar concentrations. Libraries were sequenced using single-end or pair-end reads on an Illumina NextSeq instrument using the mid-output 75 cycles.

RNA-seq data analysis

RNA-seq reads were trimmed for quality score greater than 20 and length greater than 50 using Skewer (version 0.2.2) automatically detecting adapters (*65*). Reads were mapped to the *Mabs* subsp. *abscessus* ATCC 19977 genome (NC_010397.1) using Bowtie 2 (version 2.3.5) end-to-end alignment with default parameters (*66*). Count tables were constructed from sorted BAM files using HTSeq-count (version 0.11.1) (*67*) set to non-stranded, intersection_nonempty using the gff3 file for NC_010397.1 and counting reads on gene_id. Gene expression and differential expression

analysis was completed in R (version 3.6.0) using DESeq2 (version 1.26.0) (*68*). Genes were identified as differentially expressed if they had a $\log_2$ fold change of 1 (*Mabs* WT untreated vs treated with ART or OZ439) or 2 (*Mabs* WT vs *Mabs*Δ*dosRS*) and an Benjamini-Hochberg multiple testing correction adjusted *p*- value of 0.05 or less. The sequencing data described in this publication have been submitted to the NCBI gene expression omnibus (GEO) under BioProject # PRJNA713504 and GEO accession # GSE174310.

UV-visible spectroscopy assay and mass spectrometry

A recombinant form of *Mabs* ATCC 19977 DosS (MAB_3890c) was produced in *E. coli* BL21(DE3) using the pET14b expression system (Novagen, Madison, WI) and pGro7, and purified essentially as described (*45*). Briefly, His_6–DosS expression was induced by isopropyl 1-thio-β-D-galactopyranoside (IPTG, 0.5 mM) at 16°C for 20 h. The cell pellet was suspended in lysis buffer (50 mM sodium phosphate (pH 7.6), 10% glycerol, 200 mM sodium chloride, 1% Triton X-100, 0.5 mg mL^{-1} lysozyme, 0.1 mg mL^{-1} PMSF) and the cell suspension was incubated with shaking at 37°C for 30 min prior to lysis using a French press (1400 – 1800 PSI). The soluble extract was applied to a Co^{2+} column (Clontech) and washed with washing buffers (with or without 20 mM imidazole in 50 mM sodium phosphate (pH 7.6), 10% glycerol and 500 mM sodium chloride). The recombinant protein was eluted with 200 mM imidazole in the same buffer. The fractions containing the purified protein were pooled and dialyzed in 20 mM Tris–HCl, pH 7.5. The absorption spectrum of *Mabs* DosS (5.25 μM) was analyzed as previously described (*30,45*). Briefly, 5.25 μM of purified recombinant DosS protein was deoxygenated in an anaerobic chamber (COY, 95% nitrogen – 5% hydrogen). The protein was reduced with 100 μM DTN for 20 min. The reaction was then treated with 100 μM ART, 100 μM MSU-39446, 100 μM OZ439 or an

equal volume of DMSO. The UV-visible spectra were recorded for kinetic changes over 2 h using a UV-1800 spectrophotometer (Shimadzu). The experiment was repeated at least twice with similar results.

Mouse infections and treatments

Six to eight-week-old mice were used in all experiments. Fox Chase severe combined immunodeficiency (SCID) Beige mice were ordered from Charles River (North Wilmington, MA, USA).

SCID mice were challenged with the different *Mabs* WT and recombinant strains using intravenous orinfections calibrated to deliver $1.0x10^6$ bacilli per animal. Five animals were infected for each time point. Bacterial inocula were prepared as described (*69*). At different time points post-infection, bacterial loads in the lungs, liver and spleen were determined. Bacterial counts were determined by plating serial dilutions of organ homogenates on nutrient 7H11-OADC agar (containing 0.4% charcoal in cases where mice received DosS inhibitor and antibiotic treatment) and counting colony-forming units after 5-10 d incubation at 30°C.

OZ277 and OZ439 were formulated in HPMC-SV (0.5% (w/v) hydroxy-propyl methylcellulose, 0.5% (v/v) benzyl alcohol and 0.4% (v/v) Tween 80 in milliQ water).

Tissue distribution of ozonides following *in vivo* administration

Four to eight *Mabs* ATCC 19977-infected SCID mice (2 to 4 mice per time point) having received OZ277 and OZ439 as stand-alone drugs by gavage were ethically euthanized on the last day of the experiment for comparison of drug concentrations in the plasma and lung tissues 2 and 24 h (OZ277) or 2 and 48 h (OZ439) after the last dose. For quantitation of OZ277 and OZ439 by HPLC

coupled to tandem mass spectrometry (LC-MS/MS), 1 mg mL^{-1} DMSO stock solutions of OZ277 and OZ439 were serially diluted in 50/50 acetonitrile/water to create standard curves and quality control spiking solutions. Drug-free K2EDTA plasma and lungs from CD-1 mice were obtained from BioIVT for use as blank matrices to build standard curves. Lung tissues were weighed and homogenized in 19 volumes of PBS containing 1% formic acid to 1 part tissue that was pre-chilled. Homogenization was achieved using a FastPrep-24 instrument (MP Biomedicals) and 1.4 mm zirconium oxide beads (Bertin Corp.). PBS was pre-chilled and formic acid was added to stabilize the drugs during homogenization. Spiked matrix standards and quality control (QC) samples were created by adding 10 µL of spiking solutions to 90 µL of drug-free plasma or control lung homogenate. Extraction was performed by adding 200 µL of 1:1 acetonitrile/methanol containing 10 ng mL^{-1} of the internal standard, verapamil.

LC-MS/MS analysis was performed on a Sciex Qtrap 6500 + triple-quadrupole mass spectrometer coupled to a Shimadzu Nexera X2 UHPLC system to quantify each drug in plasma. Chromatography was performed on an Agilent Zorbax SB-C8 column (2.1x30 mm; particle size, 3.5 µm) using a reverse phase gradient elution. Milli-Q deionized water with 0.1% formic acid was used for the aqueous mobile phase and 0.1% formic acid in acetonitrile for the organic mobile phase. Multiple-reaction monitoring (MRM) of precursor/fragment transitions in electrospray positive-ionization mode was used to quantify the analytes. MRM transitions of 470.24/304.00, 393.24/227.00, and 455.40/165.20 were used for OZ439, OZ277, and verapamil respectively. Sample analysis was accepted if the concentrations of the quality control samples were within 20% of the nominal concentration. Data processing was performed using Analyst software (version 1.6.3; Sciex).

Flow cytometry analysis of mCHERRY-expressing MABSC bacilli

WT *Mabs* ATCC 19977, *Mabs*Δ*dosRS* and *Mabs*Δ*dosRS* complemented with *dosRS* expressing mCherry from pCHERRY3 (Addgene # 24659) were grown under hypoxic conditions in the Wayne model. At the time the cultures reached hypoxia (d 0; i. e. 3 d post-inoculation) or after 3 weeks of incubation under hypoxia (d 21), cultures were centrifuged and the bacterial pellets were washed three times with 0.85% NaCl containing 0.05% Tween 80. Bacterial cells fixed with 2% paraformaldehyde for 1 h at room temperature and passed through a single cell strainer (40 μm) were then analyzed on a 4-laser Cytek® Aurora flow cytometer using a 561 nm excitation laser and a yellow-green detector module. Freshly-grown *Mabs* ATCC 19977 harboring or not the mCherry-expressing plasmid were used as positive and negative controls for gating, respectively.

Statistical analysis

The unpaired Student *t*-test (GraphPad Prism) was used to assess statistical significance between strains and treatment groups *in vitro* and *in vivo*.

Supplementary Materials

Fig. S1. Kinetics of expression of the *dosR* and *dosS* genes under microaerophilic conditions in WT *Mabs* ATCC 19977 and the Δ*dosRS* knock-out mutant complemented with *dosRS*.

Fig. S2. Gene replacement at the *dosRS* locus of *Mabs* ATCC 19977.

Fig. S3. Loss of viability of *Mabs*Δ*dosRS* in the Wayne model.

Fig. S4. Effect of knocking-out *dosRS* on *M. abscessus* lipid biosynthesis.

Fig. S5. Growth characteristics of *Mabs* ATCC 19977 WT, the *dosRS* KO and the *dosR* and *dosRS* complemented mutant strains in SCFM at 37°C.

Fig. S6. Effect of DosS inhibitors on the drug tolerance of *Mabs*Δ*dosRS* under hypoxia.

Fig. S7. Effect of DosS inhibitors on MABSC biofilm dispersal.

Fig. S8. Identification of the *Mabs* DosR DNA-binding site.

Fig. S9. Transcriptional profiles of ART- and OZ439-treated WT *Mabs* ATCC 19977 cells and of the *dosRS* KO mutant under microaerophilic growth conditions.

Fig. S10. Effect of DosS inhibitors on NO signaling.

Fig. S11. Therapeutic efficacy of OZ277 in acutely MABSC-infected SCID mice.

Table S1. Characterization of the DosRS regulon of *Mabs* ATCC 19977.

Table S2. [see separate Excel file]: RNA-seq dataset of differentially expressed genes in all comparisons.

Table S3. [see separate Excel file]: ssDNA oligo probes covering *Mabs* 16s and 23s rRNA used in rRNA depletion.

References and Notes

1. R. A. Floto, C. S. Haworth, The growing threat of nontuberculous mycobacteria in CF. *J Cyst Fibros* **14**, 1-2 (2015).
2. S. L. Martiniano, J. A. Nick, C. L. Daley, Nontuberculous Mycobacterial Infections in Cystic Fibrosis. *Thorac Surg Clin* **29**, 95-108 (2019).

3. I. K. Park, K. N. Olivier, Nontuberculous mycobacteria in cystic fibrosis and non-cystic fibrosis bronchiectasis. *Semin Respir Crit Care Med* **36**, 217-224 (2015).

4. M. L. Wu, D. B. Aziz, V. Dartois, T. Dick, NTM drug discovery: status, gaps and the way forward. *Drug Discov Tod* **23**, 1502-1519 (2018).

5. S. M. Holland, Nontuberculous mycobacteria. *Am J Med Sci* **321**, 49-55 (2001).

6. K. P. Fennelly, C. Ojano-Dirain, Q. Yang, L. Liu, L. Lu, A. Progulske-Fox, G. P. Wang, P. Antonelli, P., G. Schultz, Biofilm Formation by *Mycobacterium abscessus* in a Lung Cavity. *Am J Respir Crit Care Med* **193**, 692-693 (2016).

7. T. Qvist, S. Eickhardt, K. N. Kragh, C. B. Andersen, M. Iversen, N. Hoiby, T. Bjarnsholt, Chronic pulmonary disease with *Mycobacterium abscessus* complex is a biofilm infection. *Eur Respir J* **46**, 1823-1826 (2015).

8. J. F. Tomashefski Jr., R. C. Stern, C. A. Demko, C. F. Doershuk, Nontuberculous mycobacteria in cystic fibrosis. An autopsy study. *Am J Respir Crit Care Med* **154**, 523-528 (1996).

9. A. R. Cullen, C. L. Cannon, E. J. Mark, A. A. Colin, *Mycobacterium abscessus* infection in cystic fibrosis. Colonization or infection? *Am J Respir Crit Care Med* **161**, 641-645 (2000).

10. A. Viljoen, J. L. Herrmann, O. K. Onajole, J. Stec, A. P. Kozikowski, L. Kremer, Controlling Extra- and Intramacrophagic *Mycobacterium abscessus* by Targeting Mycolic Acid Transport. *Front Cell Infect Microbiol* **7**, 388 (2017).

11. L. Babrak, L. Danelishvili, S. J. Rose, L. E. Bermudez, Microaggregate-associated protein involved in invasion of epithelial cells by *Mycobacterium avium* subsp. *hominissuis*. *Virulence* **6**, 694-703 (2015).

12. L. Babrak, L. Danelishvili, S. J. Rose, T. Kornberg, L. E. Bermudez, The environment of "*Mycobacterium avium* subsp. *hominissuis*" microaggregates induces synthesis of small proteins associated with efficient infection of respiratory epithelial cells. *Infect Immun* **83**, 625-636 (2015).

13. K. C. Malcolm, E. M. Nichols, S. M. Caceres, J. E. Kret, S. L. Martiniano, S. D. Sagel, E. D. Chan, L. Caverly, G. M. Solomon, P. Reynolds, D. L. Bratton, J. L. Taylor-Cousar, D. P. Nichols, M. T. Saavedra, J. A. Nick, *Mycobacterium abscessus* induces a limited pattern of neutrophil activation that promotes pathogen survival. *PLoS One* **8**, e57402 (2013).

14. S. J. Rose, L. E. Bermudez,. *Mycobacterium avium* biofilm attenuates mononuclear phagocyte function by triggering hyperstimulation and apoptosis during early infection. *Infect Immun* **82**, 405-412 (2014).

15. Y. Yamazaki, L. Danelishvili, M. Wu, E. Hidaka, T. Katsuyama, B. Stang, M. Petrofsky, R. Bildfell, L. E. Bermudez, The ability to form biofilm influences *Mycobacterium avium* invasion and translocation of bronchial epithelial cells. *Cell Microbiol* **8**, 806-814 (2006).

16. N. A. Hoiby, short history of microbial biofilms and biofilm infections. *APMIS* **125**, 272-275 (2017).

17. G. Clary, G., S. J. Sasindran, N. Nesbitt, L. Mason, S. Cole, A. Azad, K. McCoy, L. S. Schlesinger, L. Hall-Stoodley, *Mycobacterium abscessus* Smooth and Rough Morphotypes Form Antimicrobial-Tolerant Biofilm Phenotypes but Are Killed by Acetic Acid. *Antimicrob Agents Chemother* **62** (2018).

18. A. Folkesson, L. Jelsbak, L. Yang, H. K. Johansen, O. Ciofu, N. Hoiby, S. Molin, Adaptation of *Pseudomonas aeruginosa* to the cystic fibrosis airway: an evolutionary perspective. *Nat Rev Microbiol* **10**, 841-851 (2012).

19. R. Greendyke, T. F. Byrd, Differential antibiotic susceptibility of *Mycobacterium abscessus* variants in biofilms and macrophages compared to that of planktonic bacteria. *Antimicrob Agents Chemother* **52**, 2019-2026 (2008).

20. L. Hall-Stoodley, J. W. Costerton, P. Stoodley, Bacterial biofilms: from the natural environment to infectious diseases. *Nat Rev Microbiol* **2**, 95-108 (2004).

21. M. Kolpen, P. O. Jensen, T. Qvist, K. N. Kragh, C. Ravnholt, B. G. Fritz, U. R. Johansen, T. Bjarnsholt, N. Hoiby, Biofilms of *Mycobacterium abscessus* Complex Can Be Sensitized to Antibiotics by Disaggregation and Oxygenation. *Antimicrob Agents Chemother* **64** (2020).

22. D. Lebeaux, J. M. Ghigo, C. Beloin, Biofilm-related infections: bridging the gap between clinical management and fundamental aspects of recalcitrance toward antibiotics. *Microbiol Mol Biol Rev* **78**, 510-543 (2014).

23. R. L. Leistikow, R. A. Morton, I. L. Bartek, I. Frimpong, K.Wagner, K., M. I. Voskuil, The *Mycobacterium tuberculosis* DosR regulon assists in metabolic homeostasis and enables rapid recovery from nonrespiring dormancy. *J Bacteriol* **192**, 1662-1670 (2010).

24. D. Schnappinger, S. Ehrt, M. I. Voskuil, Y. Liu, J. A. Mangan, I. M. Monahan, G. Dolganov, B. Efron, P. D. Butcher, C. Nathan, C., G. K. Schoolnik, Transcriptional Adaptation of *Mycobacterium tuberculosis* within Macrophages: Insights into the Phagosomal Environment. *J Exp Med* **198**, 693-704 (2003).

25. M. I. Voskuil, D. Schnappinger, K. C. Visconti, M. I. Harrell, G. M. Dolganov, D. R. Sherman, G. K. Schoolnik, Inhibition of respiration by nitric oxide induces a *Mycobacterium tuberculosis* dormancy program. *J Exp Med* **198**, 705-713 (2003).

26. U. S. Gautam, A. McGillivray, S. Mehra, P. J. Didier, C. C. Midkiff, R. S. Kissee, N. A. Golden, X. Alvarez, T. Niu, J. Rengarajan, D. R. Sherman, D. Kaushal, DosS Is required for the complete virulence of *Mycobacterium tuberculosis* in mice with classical granulomatous lesions. *Am J Respir Cell Mol Biol* **52**, 708-716 (2015).

27. A. Kumar, J. C. Toledo, R. P. Patel, J. R. Lancaster Jr., A. J. Steyn, *Mycobacterium tuberculosis* DosS is a redox sensor and DosT is a hypoxia sensor. *Proc Natl Acad Sci U S A* **104**, 11568-11573 (2007).

28. H. D. Park, K. M. Guinn, M. I. Harrell, R. Liao, M. I. Voskuil, M. Tompa, G. K. Schoolnik, D. R. Sherman, Rv3133c/dosR is a transcription factor that mediates the hypoxic response of *Mycobacterium tuberculosis*. *Mol Microbiol* **48**, 833-843 (2003).

29. H. Zheng, H., R. B. Abramovitch, Inhibiting DosRST as a new approach to tuberculosis therapy. *Future Med Chem* **12**, 457-467 (2020).

30. H. Zheng, J. T. Williams, B. Aleiwi, E. Ellsworth, R. B. Abramovitch, Inhibiting *Mycobacterium tuberculosis* DosRST Signaling by Targeting Response Regulator DNA Binding and Sensor Kinase Heme. *ACS Chem Biol* **15**, 52-62 (2020).

31. A. Gerasimova, A. E. Kazakov, A. P. Arkin, I. Dubchak, M. S. Gelfand, Comparative genomics of the dormancy regulons in mycobacteria. *J Bacteriol* **193**, 3446-3452 (2011).

32. A. A. Miranda-CasoLuengo, P. M. Staunton, A. M. Dinan, A. J. Lohan, B. J. Loftus, Functional characterization of the *Mycobacterium abscessus* genome coupled with condition specific transcriptomics reveals conserved molecular strategies for host adaptation and persistence. *BMC Genomics* **17**, 553 (2016).

33. A. Pawlik, G. Garnier, M. Orgeur, P. Tong, A. Lohan, F. Le Chevalier, G. Sapriel, A. L. Roux, K. Conlon, N. Honore, M. A. Dillies, L. Ma, C. Bouchier, J. Y. Coppee, J. L.

Gaillard, S. V. Gordon, B. Loftus, R. Brosch, J. L. Herrmann, Identification and characterization of the genetic changes responsible for the characteristic smooth-to-rough morphotype alterations of clinically persistent *Mycobacterium abscessus*. *Mol Microbiol* **90**, 612-629 (2013).

34. E. Catherinot, A. L. Roux, E. Macheras, D. Hubert, M. Matmar, L. Dannhoffer, T. Chinet, P. Morand, C. Poyart, B. Heym, M. Rottman, J. L. Gaillard, J. L. Herrmann, Acute respiratory failure involving an R variant of *Mycobacterium abscessus*. *J Clin Microbiol* **47**, 271-274 (2009).

35. L. G. Wayne, L. G. Hayes, An *in vitro* model for sequential study of shiftdown of *Mycobacterium tuberculosis* through two stages of non-replicating persistence. *Infect. Immun.* **64**, 2062-2069 (1996).

36. S. H. Baek, A. H. Li, C. M. Sassetti, Metabolic regulation of mycobacterial growth and antibiotic sensitivity. *PLoS Biol* **9**, e1001065 (2011).

37. J. Daniel, H. Maamar, C. Deb, T. D. Sirakova, P. E. Kolattukudy, *Mycobacterium tuberculosis* uses host triacylglycerol to accumulate lipid droplets and acquires a dormancy-like phenotype in lipid-loaded macrophages. *PLoS Pathog* **7**, e1002093 (2011).

38. C. Deb, C. M. Lee, V. S. Dubey, J. Daniel, B. Abomoelak, T. D. Sirakova, S. Pawar, L. Rogers, P. E. Kolattukudy, A novel *in vitro* multiple-stress dormancy model for *Mycobacterium tuberculosis* generates a lipid-loaded, drug-tolerant, dormant pathogen. *PLoS One* **4**, e6077 (2009).

39. J. M. Belardinelli, W. Li, C. Avanzi, S. K. Angala, E. Lian, C. J. Wiersma, Z. Palčeková, K. H. Martin, B. Angala, V. C. N. de Moura, C. Kerns, V. Jones, M. Gonzalez-Juarrero, R. M. Davidson, J. A. Nick, B. R. Borlee, M. Jackson, Unique features of *Mycobacterium*

abscessus biofilms formed in synthetic cystic fibrosis medium. *Front Microbiol* **12**, 743126 (2021).

40. C. J. Wiersma, J. M. Belardinelli, C. Avanzi, S. K. Angala, I. Everall, B. Angala, E. Kendall, V. C. N. de Moura, D. Verma, J. Benoit, K. P. Brown, V. Jones, K. C. Malcolm, M. Strong, J. A. Nick, R. A. Floto, J. Parkhill, D. J. Ordway, R. M. Davidson, M. R. McNeil, M. Jackson, Cell Surface Remodeling of *Mycobacterium abscessus* under Cystic Fibrosis Airway Growth Conditions. *ACS Infect Dis* **6**, 2143-2154 (2020).

41. E. Rampacci, V. Stefanetti, V., F. Passamonti, M. Henao-Tamayo, Preclinical Models of Nontuberculous Mycobacteria Infection for Early Drug Discovery and Vaccine Research. *Pathogens* **9** (2020).

42. Y. K. Yam, N. Alvarez, M. L. Go, T. Dick, Extreme Drug Tolerance of *Mycobacterium abscessus* "Persisters". *Front Microbiol* **11**, 359 (2020).

43. E. C. Maggioncalda, E. Story-Roller, J. Mylius, P. Illei, R. J. Basaraba, G. Lamichhane, A mouse model of pulmonary *Mycobacteroides abscessus* infection. *Sci Rep* **10**, 3690 (2020).

44. A. Obregon-Henao, K. A. Arnett, M. Henao-Tamayo, L. Massoudi, E. Creissen, K. Andries, A. J. Lenaerts, D. J. Ordway, Susceptibility of *Mycobacterium abscessus* to antimycobacterial drugs in preclinical models. *Antimicrob Agents Chemother* **59**, 6904-6912 (2015).

45. H. Zheng, C. J. Colvin, B. K. Johnson, P. D. Kirchhoff, M. Wilson, K. Jorgensen-Muga, S. D. Larsen, R. B. Abramovitch, Inhibitors of *Mycobacterium tuberculosis* DosRST signaling and persistence. *Nat Chem Biol* **13**, 218-225 (2017).

46. S. A. Charman, S. Arbe-Barnes, I. C. Bathurst, R. Brun, M. Campbell, W. N. Charman, F. C. Chiu, J. Chollet, J. C. Craft, D. J. Creek, Y. Dong, H. Matile, M. Maurer, J. Morizzi, T.

Nguyen, P. Papastogiannidis, C. Scheurer, D. M. Shackleford, K. Sriraghavan, L. Stingelin, Y. Tang, H. Urwyler, X. Wang, K. L. White, S. Wittlin, L. Zhou, J. L. Vennerstrom, Synthetic ozonide drug candidate OZ439 offers new hope for a single-dose cure of uncomplicated malaria. *Proc Natl Acad Sci U S A* **108**, 4400-4405 (2011).

47. Y. Dong, X. Wang, S. Kamaraj, V. J. Bulbule, F. C. Chiu, J. Chollet, M. Dhanasekaran, C. D. Hein, P. Papastogiannidis, J. Morizzi, D. M. Shackleford, H. Barker, E. Ryan, C. Scheurer, Y. Tang, Q. Zhao, L. Zhou, K. L. White, H. Urwyler, W. N. Charman, H. Matile, S. Wittlin, S. A. Charman, J. L. Vennerstrom, Structure-Activity Relationship of the Antimalarial Ozonide Artefenomel (OZ439). *J Med Chem* **60**, 2654-2668 (2017).

48. J. J. Moehrle, S. Duparc, C. Siethoff, P. L.van Giersbergen, J. C. Craft, S. Arbe-Barnes, S. A. Charman, M. Gutierrez, S. Wittlin, J. L. Vennerstrom, First-in-man safety and pharmacokinetics of synthetic ozonide OZ439 demonstrates an improved exposure profile relative to other peroxide antimalarials. *Br J Clin Pharmacol* **75**, 524-537 (2013).

49. N. Valecha, S. Looareesuwan, A. Martensson, S. M. Abdulla, S. Krudsood, N. Tangpukdee, S. Mohanty, S. K. Mishra, P. K. Tyagi, S. K. Sharma, J. Moehrle, A. Gautam, A. Roy, J. K. Paliwal, M. Kothari, N. Saha, A. P. Dash, A.Bjorkman, Arterolane, a new synthetic trioxolane for treatment of uncomplicated *Plasmodium falciparum* malaria: a phase II, multicenter, randomized, dose-finding clinical trial. *Clin Infect Dis* **51**, 684-691 (2010).

50. T. N. Wells, R. Hooft van Huijsduijnen, W. C. Van Voorhis, Malaria medicines: a glass half full? *Nat Rev Drug Discov* **14**, 424-442 (2015).

51. S. Selvaraj, V. Sambandam, D. Sardar, S. Anishetty, In silico analysis of DosR regulon proteins of *Mycobacterium tuberculosis*. *Gene* **506**, 233-241 (2012).

52. Y. M. Chuang, N. K. Dutta, C. F. Hung, T. C. Wu, H. Rubin, P. C. Karakousis, Stringent Response Factors PPX1 and PPK2 Play an Important Role in *Mycobacterium tuberculosis* Metabolism, Biofilm Formation, and Sensitivity to Isoniazid In Vivo. *Antimicrob Agents Chemother* **60**, 6460-6470 (2016).

53. S. N. Doddam, V. Peddireddy, P. Yerra, P. P. Sai Arun, M. A. Qaria, R. Baddam, N. Sarker, N. Ahmed, *Mycobacterium tuberculosis* DosR regulon gene Rv2004c contributes to streptomycin resistance and intracellular survival. *Int J Med Microbiol* **309**, 151353 (2019).

54. D. Sharma, M. Lata, M. Faheem, A. U. Khan, B. Joshi, K. Venkatesan, S. Shukla, D. Bisht, Role of *M. tuberculosis* protein Rv2005c in the aminoglycosides resistance. *Microb Pathog* **132**, 150-155 (2019).

55. A. Venugopal, R. Bryk, S. Shi, K. Rhee, P. Rath, D. Schnappinger, S. Ehrt, C. Nathan, Virulence of *Mycobacterium tuberculosis* depends on lipoamide dehydrogenase, a member of three multienzyme complexes. *Cell Host Microbe* **9**, 21-31 (2011).

56. T. A. Hudock, T. W. Foreman, N. Bandyopadhyay, U. S. Gautam, A. V. Veatch, D. N. LoBato, K. M. Gentry, N. A. Golden, A. Cavigli, M. Mueller, S. A. Hwang, R. L. Hunter, X. Alvarez, A. A. Lackner, J. S. Bader, S. Mehra, D. Kaushal, Hypoxia Sensing and Persistence Genes Are Expressed during the Intragranulomatous Survival of *Mycobacterium tuberculosis*. *Am J Respir Cell Mol Biol* **56**, 637-647 (2017).

57. S. Mehra, T. W. Foreman, P. J. Didier, M. H. Ahsan, T. A. Hudock, R. Kissee, N. A. Golden, U. S. Gautam, A. M. Johnson, X. Alvarez, K. E. Russell-Lodrigue, L. A. Doyle, C. J. Roy, T. Niu, J. L. Blanchard, S. A. Khader, A. A. Lackner, D. R. Sherman, D. Kaushal, The DosR Regulon Modulates Adaptive Immunity and Is Essential for *Mycobacterium tuberculosis* Persistence. *Am J Respir Crit Care Med* **191**, 1185-1196 (2015).

58. U. S. Gautam, S. Mehra, P. Kumari, X. Alvarez, T. Niu, J. S. Tyagi, D. Kaushal,. *Mycobacterium tuberculosis* sensor kinase DosS modulates the autophagosome in a DosR-independent manner. *Commun Biol* **2**, 349 (2019).

59. E. Konstat-Korzenny, J. A. Ascencio-Aragon, S. Niezen-Lug, R. Vazquez-Lopez, Artemisinin and Its Synthetic Derivatives as a Possible Therapy for Cancer. *Med Sci (Basel)* **6** (2018).

60. X. Sun, P. Yan, C. Zou, Y. K. Wong, Y. Shu, Y. M. Lee, C. Zhang, N. D. Yang, J. Wang, J. Zhang, Targeting autophagy enhances the anticancer effect of artemisinin and its derivatives. *Med Res Rev* **39**, 2172-2193 (2019).

61. A. Rominski, A. Roditscheff,P. Selchow, E. C. Bottger, P. Sander, Intrinsic rifamycin resistance of *Mycobacterium abscessus* is mediated by ADP-ribosyltransferase MAB_0591. *J Antimicrob Chemother* **72**, 376-384 (2017).

62. K. H.Turner, A. K. Wessel, G. C. Palmer, J. L. Murray, M. Whiteley, Essential genome of *Pseudomonas aeruginosa* in cystic fibrosis sputum. *Proc Natl Acad Sci U S A* **112**, 4110-4115 (2015).

63. A. Martin, M. Camacho, F. Portaels, J. C. Palomino, Resazurin microtiter assay plate testing of *Mycobacterium tuberculosis* susceptibilities to second-line drugs: rapid, simple, and inexpensive method. *Antimicrob. Agents Chemother* **47**, 3616-3619 (2003).

64. Y. Huang, R. U. Sheth, A. Kaufman, H. H. Wang, Scalable and cost-effective ribonuclease-based rRNA depletion for transcriptomics. *Nucleic Acids Res* **48**, e20 (2020).

65. H. Jiang, R. Lei, S. W. Ding, S. Zhu, Skewer: a fast and accurate adapter trimmer for next-generation sequencing paired-end reads. *BMC Bioinformatics* **15**, 182 (2014).

66. B. Langmead, S. L. Salzberg, Fast gapped-read alignment with Bowtie 2. *Nat Methods* **9**, 357-359 (2012).

67. S. Anders, P. T. Pyl, W. Huber, HTSeq-a Python framework to work with high-throughput sequencing data. *Bioinformatics* **31**, 166-169 (2015).

68. M. I. Love, W. Huber, S. Anders, Moderated estimation of fold change and dispersion for RNA-seq data with DESeq2. *Genome Biol* **15** (2014).

69. B. Banaschewski, D. Verma, L. J. Pennings, M. Zimmerman, Q. Ye, J. Gadawa, V. Dartois, D. Ordway, J. van Ingen, S. Ufer, K. Stapleton, T. Hofmann, Clofazimine inhalation suspension for the aerosol treatment of pulmonary nontuberculous mycobacterial infections. *J Cyst Fibros* **18**, 714-720 (2019).

70. G. E. Crooks, G. Hon, J. M. Chandonia, S. E. Brenner, WebLogo: a sequence logo generator. *Genome Res* **14**, 1188-1190 (2004).

Acknowledgments:

We thank Dr. Peter Sander (University of Zurich, Switzerland) for the kind gift of plasmid pKH-aac(3)IVDsRed2-KatG-rpsL^{WT} and the Colorado State University Next Generation Sequencing Core for assistance with RNA-seq analyses. We thank Melanie Boersma, Myles Beaumont and Sam Sorenson for their help with biofilm staining.

Funding:

This work was supported by a research grant from the Cystic Fibrosis Foundation (to MJ and DJO), and the National Institutes of Health/ National Institute of Allergy and Infectious Diseases grants

AI147326 (to MJ and DJO), 1 S10 RR023735 (Zeiss LSM 510 Laser Scanning Microscope; to MGJ), and 1 S10 OD025127 (Keyence fluorescence microscope; CSU Microscope Imaging Network). JMB is the recipient of a Vertex Research Innovation Award. CA is supported by the European Union's Horizon 2020 research and innovation program under the Marie Sklodowska-Curie grant No 845479. The content is solely the responsibility of the authors and does not necessarily represent the official views of the sponsors.

Author Contributions:

JMB, DJO, TNCW, SAC, VD, MZ, JLV, JAN, RBA, and MJ designed the study and analyzed data. JMB, DV, WL, CA, CJW, BKJ, HW, JTW, MZ, BA, VJ, VCNM, MGJ, CP, KCM, BKP, ARS performed experiments. JLV provided critical reagents. MJ administered the project and wrote the manuscript with input from all authors.

Competing interests: JLV is an inventor on patents covering the synthetic peroxides which are owned by Medicines for Malaria Venture, where TW is an employee. RBA is the founder and owner of Tarn Biosciences, Inc., a company that is working to develop new TB drugs. RBA and BKJ are inventors on a patent application on using DosRS inhibitors to treat mycobacterial infections (application number 16/339,896). RBA is the inventor on a patent application for using HC106 analogs as DosRS inhibitors to treat mycobacterial infections (application number 16/955,385).

Data and Materials Availability: The sequencing data described in this publication have been submitted to the NCBI gene expression omnibus (GEO) under BioProject # PRJNA713504 and

GEO accession # GSE174310. Other data are available in the main text or the supplementary materials. Materials are available upon request and are subject to a Material Transfer Agreement.

Figures legends

Fig. 1: DosRS is required for the adaptation and drug tolerance of *M. abscessus* under hypoxia.

(**A**) Quantitative reverse-transcription PCR showing a strong upregulation of the *dosR* gene in *Mabs* ATCC 19977 grown for 24 h under microaerophilic conditions in standing T25 vented tissue culture flasks compared to well-aerated shaking flasks. DosR cDNA was normalized internally to the *sigA* cDNA in the same sample and the *dosR* mRNA level under microaerophilic conditions is expressed relative to the mRNA level of this gene under oxygenated conditions arbitrarily set to 1. Ratios of *dosR*/*sigA* mRNA are means ± SD (n = 3 RNA extractions and RT-qPCR reactions). (**B**) Comparative survival curves of the WT, *dosRS* mutant and the *dosR* and *dosRS* complemented mutant strains in the Wayne model. Decolorization of methylene blue occurred on d 5 indicative of oxygen depletion. The results presented are the means (± SD) of triplicate cultures and are representative of two independent experiments. Asterisks denote statistically significant differences between culture conditions pursuant to the Student's *t*-test (*$p < 0.05$; ***$p<0.0005$). (**C**) Following 5 d of culture in the Wayne model, treatment with AMK (64 μg mL^{-1}), AZI (32 μg mL^{-1}) and CFZ (2 μg mL^{-1}) for 7 d reduces the viability of the *dosRS* knock-out mutant but not that of the WT and *dosRS* complemented mutant strains. Treatment with IMI (32 μg mL^{-1}) did not reduce the viability of WT or mutant strains. The results presented are the means (± SD) of triplicate cultures from one experiment and are representative of two independent experiments. Asterisks denote statistically significant differences between culture conditions pursuant to the Student's *t*-test (*$p < 0.05$; **$p < 0.005$).

Fig. 2: Impact of DosRS deficiency on *M. abscessus* biofilm formation.

Biofilm formation after 5 d of growth in SCFM medium in poly-D-lysine-coated microplates was determined by crystal violet staining (**A**) and CFU counting (**B**). The means and standard deviations of triplicate wells are shown. Asterisks denote statistically significant differences between WT and recombinant strains as determined by the Student's *t*-test (**p < 0.005). (**C**) 2.5D rendering of the biofilms formed by WT *Mab*s ATCC 19977, *Mabs*Δ*dosRS* and the *dosRS* complementant expressing mCherry as imaged with fluorescence confocal microscopy. (**D**) Side view (XZ) of the biofilms formed by WT *Mab*s ATCC 19977, *Mabs*Δ*dosRS* and the *dosRS* complementant expressing mCherry as imaged using a KEYENCE BZ-X700 fluorescence microscope. (**E**) Biofilm thickness for each strain as measured after 5 d of growth in SCFM by 3D confocal imaging. Shown are the means and standard deviations of triplicate wells. Asterisks denote statistically significant differences between WT and recombinant strains pursuant to the Student's *t*-test (**p < 0.005). All results are representative of two to three independent experiments.

Fig. 3: Infection of SCID mice with *Mabs* ATCC 19977 WT, the *dosRS* KO mutant and the *dosRS* complemented mutant.

SCID mice were infected intravenously with $1.0x10^6$ CFU per animal of either *Mabs* ATCC 19977 WT, the *dosRS* KO mutant or the *dosRS* complemented mutant. AMK and AZI treatment of each group of mice began 28 d after infection, upon establishment of chronic infection. As of d 28, mice were treated daily (7 d/week) for 28 d with saline (gavage), AMK (150 mg/kg, subcutaneous injection) or AZI (200 mg/kg, gavage). Groups of mice were ethically euthanized on d 2, 28 and 56, and lungs and spleens were taken for bacterial enumeration (CFU). For each bacterial strain, the CFU results represent the average of 5 mice per time point, and bacterial loads are expressed

as Log_{10} CFU (± SEM). Asterisks denote statistically significant differences between antibiotic-treated WT and mutant- or complemented mutant-infected mice pursuant to the Student's *t*-test ($p^* < 0.05$; $p^{**} < 0.005$).

Fig. 4: Effect of DosS inhibitors on MABSC survival and drug tolerance under hypoxia.

(**A**) Structures of the DosS inhibitors used in this study.

(**B**) Comparative survival of the WT, *dosRS* mutant and *dosRS* complemented mutant exposed to ART and OZ439 (40 μM each) in the Wayne model. Decolorization of methylene blue occurred on d 5 indicative of oxygen depletion. DosS inhibitor treatment was applied from the time of inoculation. CFU were plated for counting 7 d after the onset of hypoxia. The results presented are the means (± SD) of triplicate cultures and are representative of two independent experiments. Asterisks denote statistically significant differences between inhibitor-treated and non-treated cultures pursuant to the Student's *t*-test (**$p < 0.005$; ***$p < 0.0005$).

(**C**) *Mabs* ATCC 19977 WT was cultured in the Wayne model in the presence of ART or OZ439 (40 μM each) from the time of inoculation. As cultures reached hypoxia, antibiotics, and more DosS inhibitors (40 μM each) were added and the cultures were incubated for another 7 d prior to CFU plating. The results presented are the means (± SD) of triplicate cultures and are representative of two independent experiments. Asterisks denote statistically significant differences between inhibitor-treated and non-treated cultures pursuant to the Student's *t*-test (*$p < 0.05$; **$p < 0.005$).

Fig. 5: Effect of DosS inhibitors on MABSC biofilm formation.

(**A**) Biofilm formation of ART-, AS-, OZ439- and OZ277-treated WT *Mabs* ATCC 19977 cultures after 5 d of growth in SCFM medium in poly-D-lysine-coated microplates as determined by crystal

violet staining. The DosS inhibitors were added to the culture medium at the indicated concentrations on the first day and maintained throughout the duration of the experiment. The results presented are the means (± SD) of quadruplicate wells from one experiment and are representative of three independent experiments. Asterisks denote statistically significant differences between inhibitor-treated and non-treated cultures pursuant to the Student's *t*-test (*p < 0.05; **p < 0.005; ***p < 0.0005; ****p < 0.00005).

(**B**) 2.5D rendering of biofilms formed by WT *Mabs* ATCC 19977 cultures either untreated or treated with ART (100 μM), OZ277 (25 or 100 μM) or OZ439 (25 or 100 μM) after 5 d of growth in SCFM.

(**C**) Biofilm thickness of untreated and inhibitor-treated WT *Mabs* ATCC 19977 as measured after d 5 of growth in SCFM by 3D confocal imaging. Shown are the means and standard deviations of triplicate wells. Asterisks denote statistically significant differences between untreated and inhibitor-treated cultures pursuant to the Student's *t*-test (*p<0.05, **p<0.005, ***p<0.001). ART, artemisinin; ARS, artesunate.

Fig. 6: Effect of disrupting *dosRS* and of *dosS* inhibitor treatment on the transcriptional profile of *Mabs* ATCC 19977.

(**A**) Differential gene expression between *Mabs* ATCC 19977 and *Mabs*Δ*dosRS* under microaerophilic conditions. Values are expressed as $\log_2$ FC vs counts per million (CPM). Genes in red have a *p*-value < 0.05 and the differential expression of five of them was further confirmed by RT-qPCR (see Fig. S9).

(**B**) Venn-diagram showing genes downregulated in *Mabs* ATCC 19977 WT by ART or OZ439 treatment ($\log_2$FC<-1, p-value<0.05) compared to genes downregulated under microaerophilic

conditions in *Mabs*Δ*dosRS* ($log_2FC<-2$, p-value<0.05). The complete list of these genes is provided in Table S2.

Fig. 7: Inhibition of the sensor kinase heme of DosS by ART, OZ439 and MSU-39446.

UV-visible spectra of DosS showing treatment with dithionite (DTN) reduces the heme, which is the "on" state for the kinase. ART, OZ439 and MSU-39446, but not the degassed DMSO control, oxidize the heme.

Fig. 8: Therapeutic efficacy and adjunct therapeutic efficacy of OZ439 in acutely and chronically MABSC-infected SCID mice.

(**A**) Exposure of OZ439 in *Mabs* ATCC 19977-infected SCID mice. In the acute model, mice received OZ439 orally (200 mg/kg) every other d for 14 d. In the chronic model, mice received OZ439 orally (50 mg/kg) every other d for 28 d. Shown are the averages (± SD) of lung and plasma concentrations 2 and 48 hs after the last dosing. Two mice were used per time point in the acute model. Four mice were used per time point in the chronic model.

(**B**) Therapeutic efficacy testing in an acute SCID mouse model of MABSC infection. Mice (n=5 mice/group) were infected intratracheally with $1.0x10^6$ CFUs of WT *Mabs* ATCC 19977. On d 12 post-infection, during the acute phase of infection, mice were treated daily (7 d/week) for 14 d, or every other day for OZ439, with vehicle used in the formulation of OZ439 (HPMC-SV), OZ439, AMK, AZI, IMI, CFZ, and the same four antibiotic treatments in combination with OZ439. See text for more details about the treatments. Bacterial loads were determined in the lungs, liver and spleen on d 2, 12 and 26.

(**C**) Therapeutic efficacy testing in a chronic SCID mouse model of MABSC infection. Mice (five animals per group) were infected intravenously with $1.0x10^6$ CFUs of WT *Mabs* ATCC 19977.

On d 28 post-infection, upon establishment of chronic infection, mice were treated daily (7 d/ week) for 28 d, or every other day for OZ439, with formulation vehicle, OZ439, AMK, AZI, IMI and CFZ, and the same four antibiotics in combination with OZ439. See text for more details about the treatments. Bacterial loads were determined in the lungs, liver, and spleen on d 2, 28 and 56. In (**B**) and (**C**), asterisks denote statistically significant differences between antibiotic-treated and antibiotic+OZ439-treated mice, or untreated and OZ439-treated mice pursuant to the Student's *t*-test (*$p < 0.05$; **$p < 0.005$; ***$p < 0.0005$).

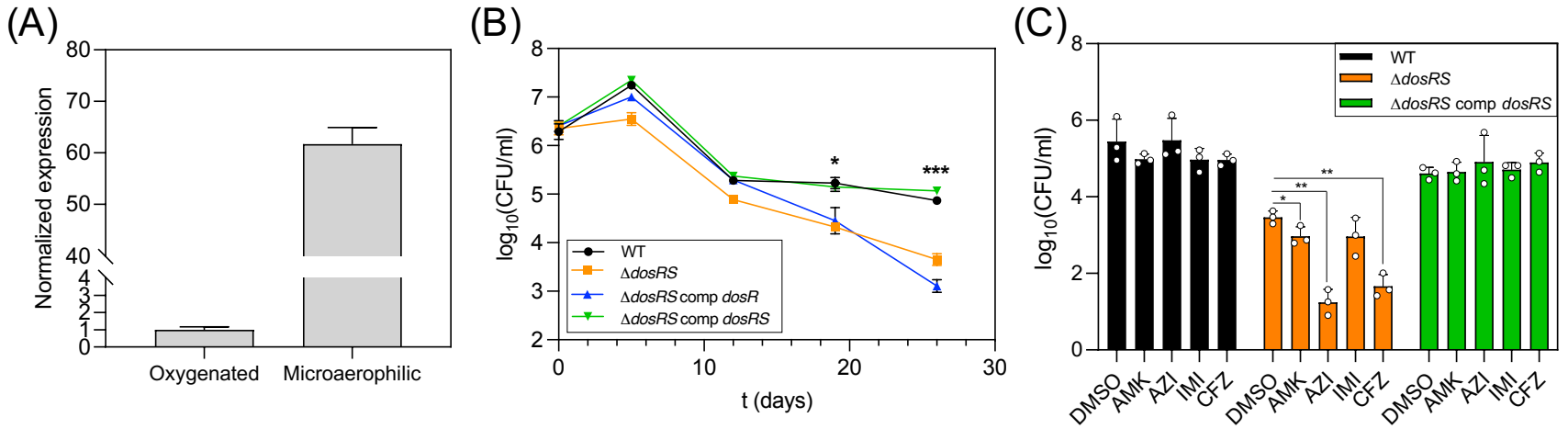
(A)
Normalized expression
Oxygenated
Microaerophilic
(B)
log10(CFU/ml)
t (days)
WT
ΔdosRS
ΔdosRS comp dosR
ΔdosRS comp dosRS
*
***
(C)
log10(CFU/ml)
WT
ΔdosRS
ΔdosRS comp dosRS
DMSO
AMK
AZI
IMI
CFZ

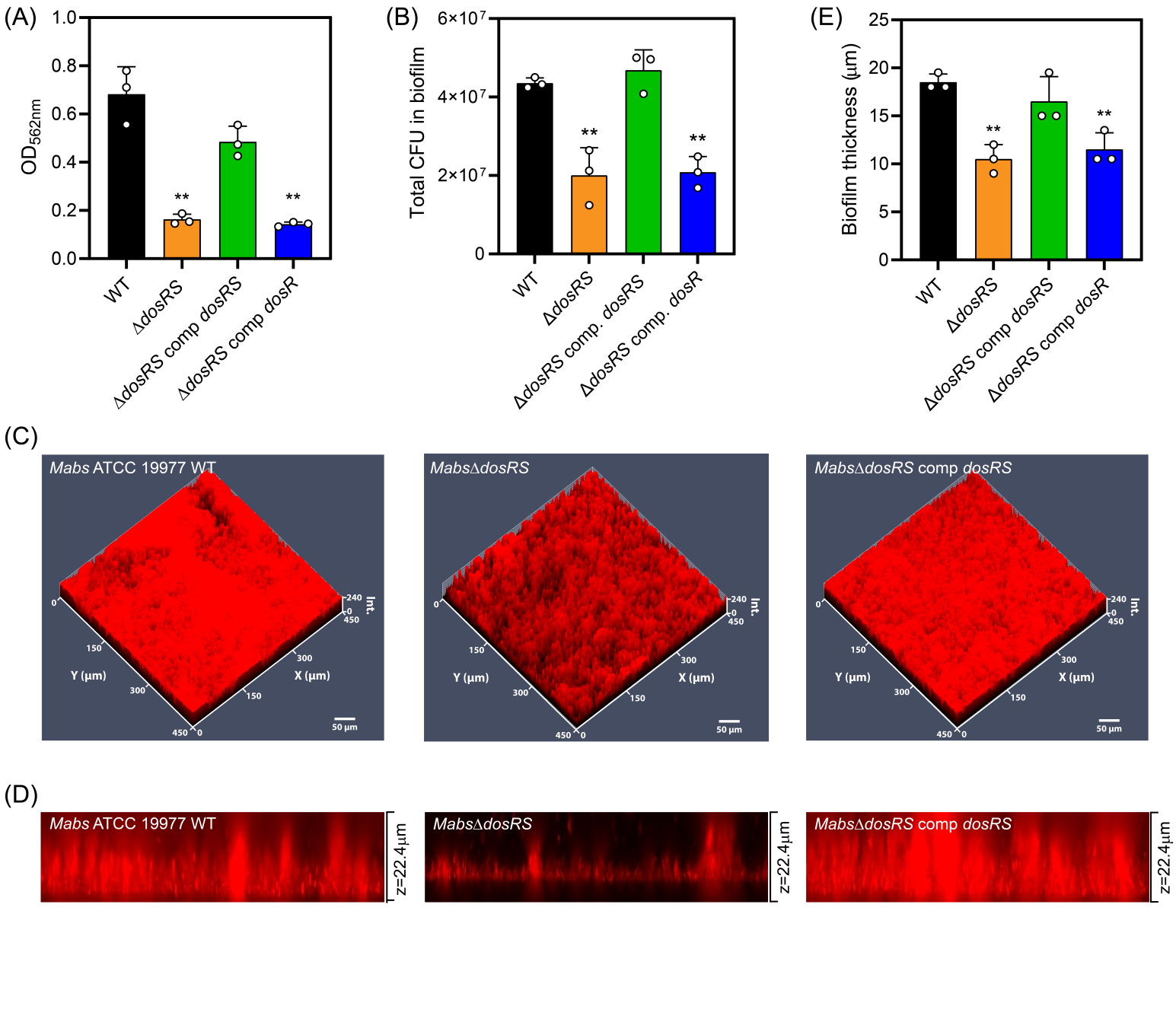
(A)
1.0
0.8
0.6
0.4
0.2
0.0
OD562nm
**
**
WT
ΔdosRS
ΔdosRS comp dosRS
ΔdosRS comp dosR
(B)
6×10^7
4×10^7
2×10^7
0
Total CFU in biofilm
**
**
WT
ΔdosRS
ΔdosRS comp. dosRS
ΔdosRS comp. dosR
(E)
25
20
15
10
5
0
Biofilm thickness (µm)
**
**
WT
ΔdosRS
ΔdosRS comp dosRS
ΔdosRS comp dosR
(C)
Mabs ATCC 19977 WT
MabsΔdosRS
MabsΔdosRS comp dosRS
Y (µm)
X (µm)
Int.
50 µm
(D)
Mabs ATCC 19977 WT
MabsΔdosRS
MabsΔdosRS comp dosRS
z=22.4µm

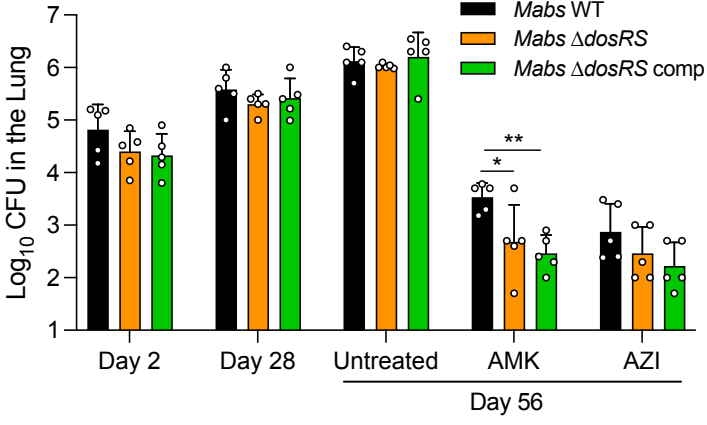
Mabs WT
Mabs ΔdosRS
Mabs ΔdosRS comp
Log10 CFU in the Lung
7
6
5
4
3
2
1
**
*
Day 2
Day 28
Untreated
AMK
AZI
Day 56

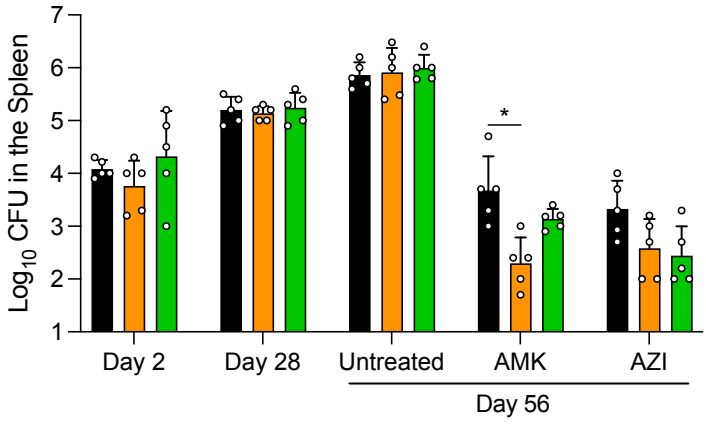
Log10 CFU in the Spleen
7
6
5
4
3
2
1
*
Day 2
Day 28
Untreated
AMK
AZI
Day 56

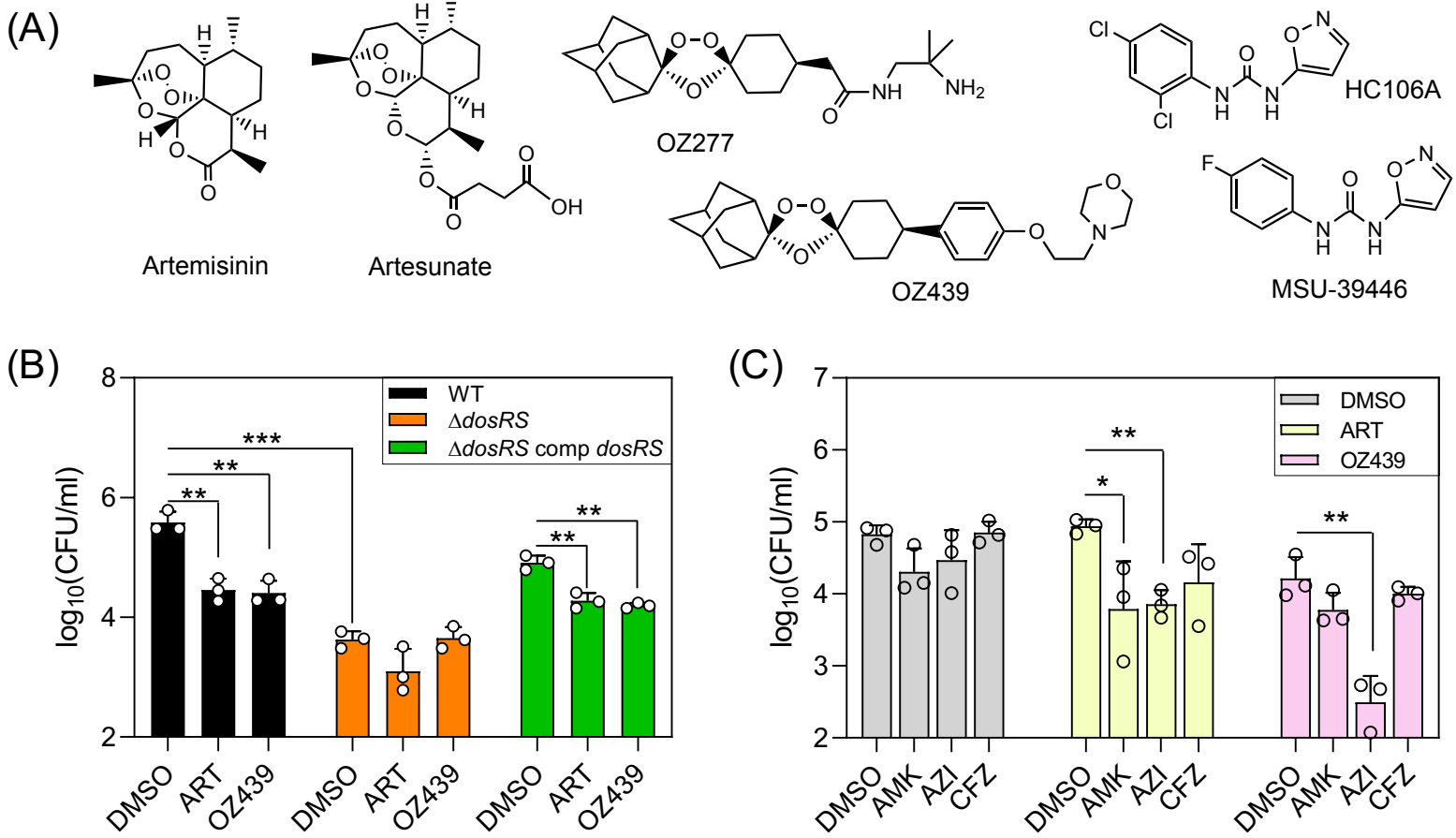
(A)
Artemisinin
Artesunate
OZ277
OZ439
HC106A
MSU-39446
(B)
log10(CFU/ml)
WT
ΔdosRS
ΔdosRS comp dosRS
DMSO
ART
OZ439
(C)
log10(CFU/ml)
DMSO
ART
OZ439
DMSO
AMK
AZI
CFZ

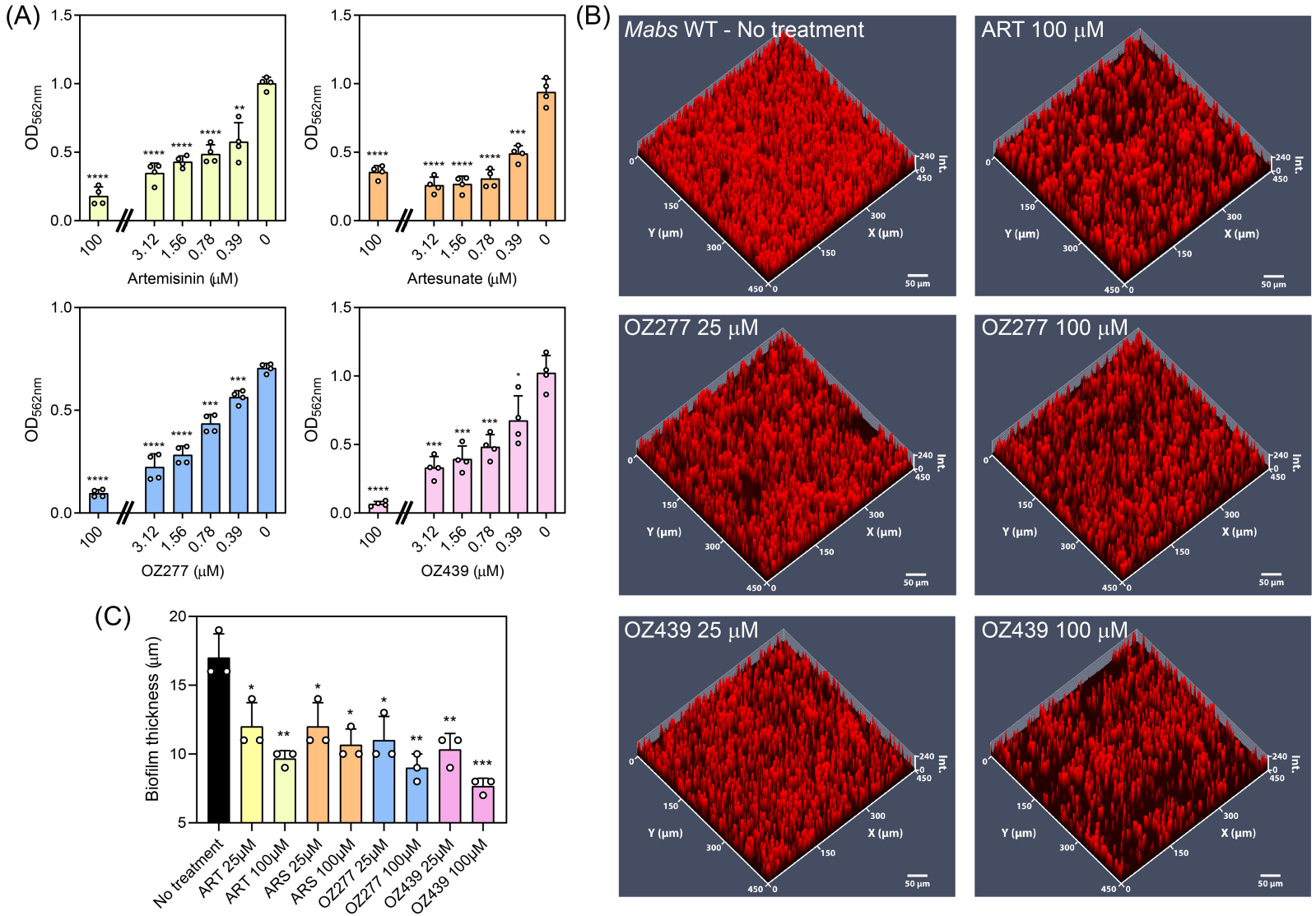
(A)
OD562nm
Artemisinin (μM)
Artesunate (μM)
OZ277 (μM)
OZ439 (μM)
100
3.12
1.56
0.78
0.39
0
(B)
Mabs WT - No treatment
ART 100 μM
OZ277 25 μM
OZ277 100 μM
OZ439 25 μM
OZ439 100 μM
Y (μm)
X (μm)
Int.
50 μm
(C)
Biofilm thickness (μm)
No treatment
ART 25μM
ART 100μM
ARS 25μM
ARS 100μM
OZ277 25μM
OZ277 100μM
OZ439 25μM
OZ439 100μM

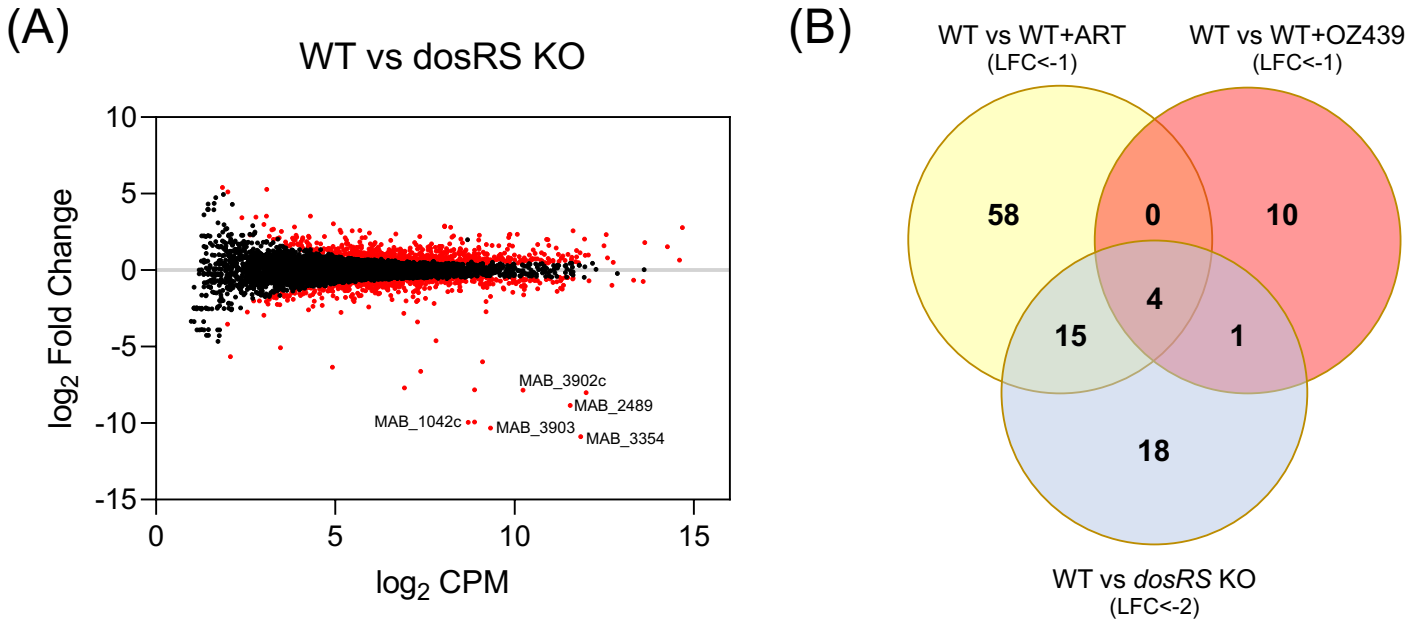
(A)
WT vs dosRS KO
log2 Fold Change
log2 CPM
10
5
0
-5
-10
-15
0
5
10
15
MAB_3902c
MAB_2489
MAB_1042c
MAB_3903
MAB_3354
(B)
WT vs WT+ART
(LFC<-1)
WT vs WT+OZ439
(LFC<-1)
58
0
10
4
15
1
18
WT vs dosRS KO
(LFC<-2)

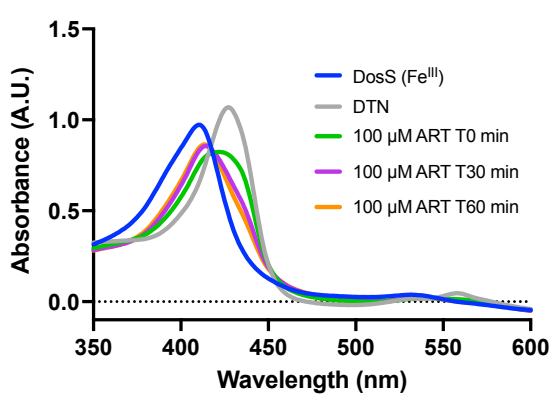
Absorbance (A.U.)
1.5
1.0
0.5
0.0
350
400
450
500
550
600
Wavelength (nm)
DosS (Fe^{III})
DTN
100 µM ART T0 min
100 µM ART T30 min
100 µM ART T60 min

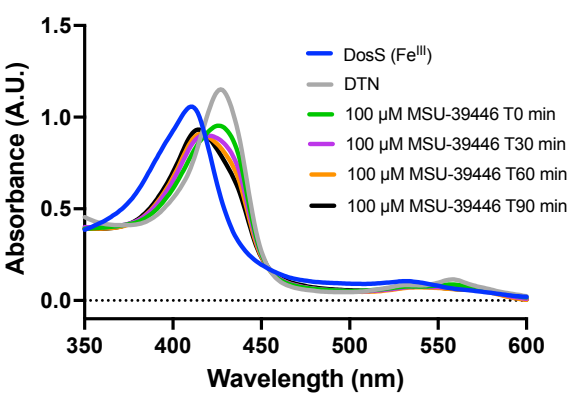
Absorbance (A.U.)
1.5
1.0
0.5
0.0
350
400
450
500
550
600
Wavelength (nm)
DosS (Fe^{III})
DTN
100 µM MSU-39446 T0 min
100 µM MSU-39446 T30 min
100 µM MSU-39446 T60 min
100 µM MSU-39446 T90 min

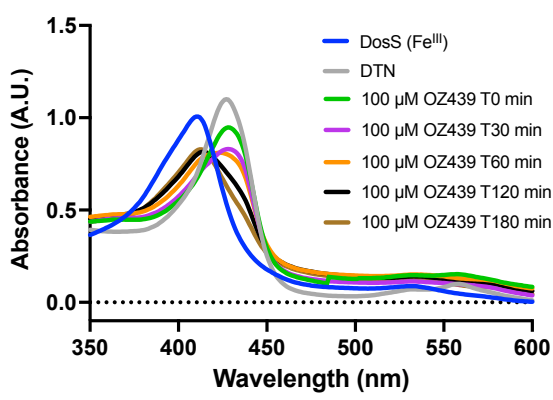
Absorbance (A.U.)
1.5
1.0
0.5
0.0
350
400
450
500
550
600
Wavelength (nm)
DosS (Fe^{III})
DTN
100 µM OZ439 T0 min
100 µM OZ439 T30 min
100 µM OZ439 T60 min
100 µM OZ439 T120 min
100 µM OZ439 T180 min

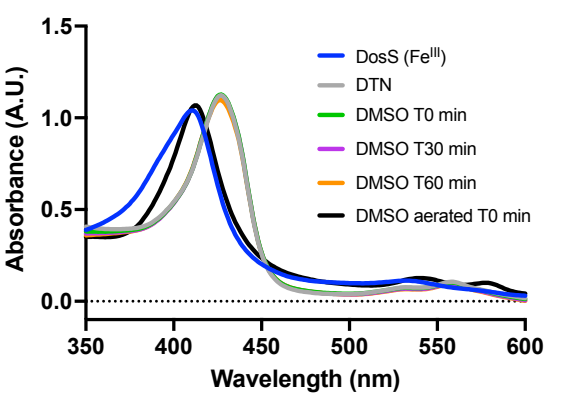
Absorbance (A.U.)
1.5
1.0
0.5
0.0
350
400
450
500
550
600
Wavelength (nm)
DosS (Fe^{III})
DTN
DMSO T0 min
DMSO T30 min
DMSO T60 min
DMSO aerated T0 min

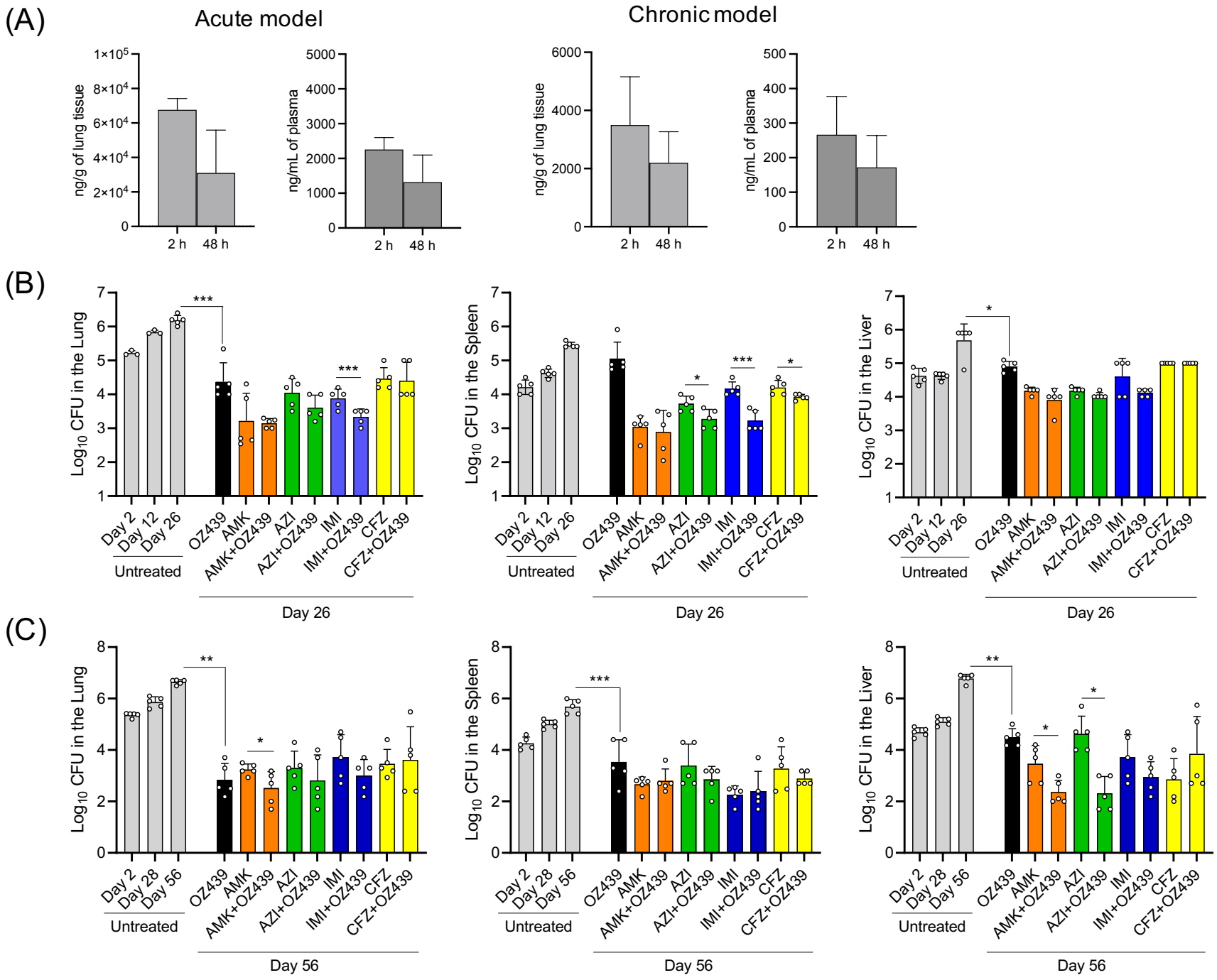
(A)
Acute model
Chronic model
ng/g of lung tissue
ng/mL of plasma
2 h
48 h
(B)
Log10 CFU in the Lung
Log10 CFU in the Spleen
Log10 CFU in the Liver
Day 2
Day 12
Day 26
Untreated
OZ439
AMK
AMK+OZ439
AZI
AZI+OZ439
IMI
IMI+OZ439
CFZ
CFZ+OZ439
Day 26
(C)
Day 2
Day 28
Day 56
Day 56

Supplementary Materials

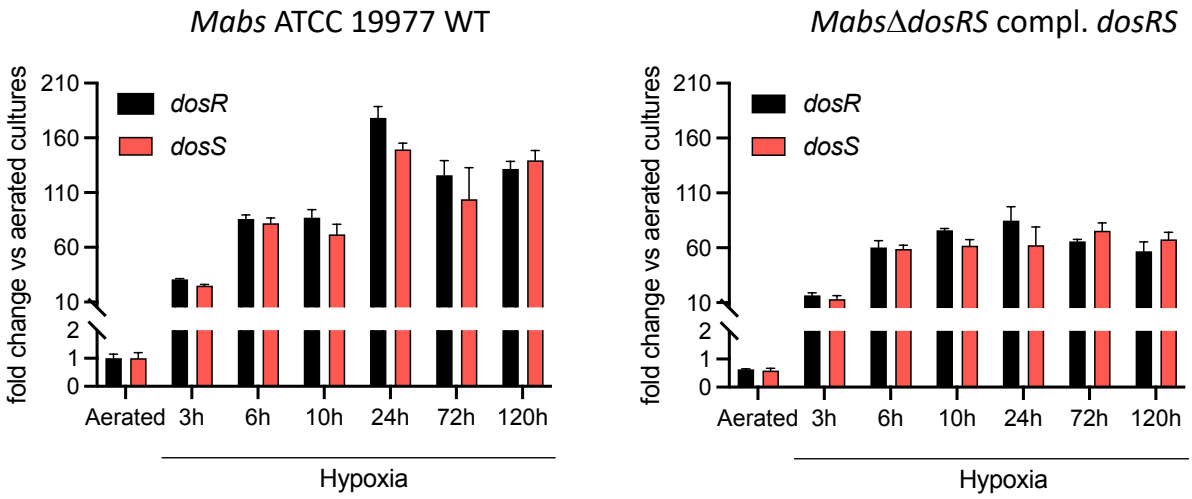

Fig. S1: Kinetics of expression of the *dosR* and *dosS* genes under microaerophilic conditions in WT *Mabs* ATCC 19977 and the Δ*dosRS* knock-out mutant complemented with *dosRS*. Quantitative reverse-transcription PCR showing a strong upregulation of the *dosR* and *dosS* genes in *Mabs* ATCC 19977 (WT strain: left panel; Δ*dosRS* mutant complemented with *dosRS*: right panel) grown under microaerophilic conditions in standing T25 vented tissue culture flasks compared to well-aerated shaking flasks, with the expression of both genes peaking in the WT strain after 24 hours. DosR and DosS cDNA was normalized internally to the *sigA* cDNA in the same sample and the *dosR* and *dosS* mRNA levels under microaerophilic conditions are expressed relative to the mRNA level of these genes under oxygenated conditions after 3 hours of incubation arbitrarily set to 1. Ratios of *dosR*/*sigA* and *dosS*/*sigA* mRNA are means ± SD (n = 3 RNA extractions and RT-qPCR reactions).

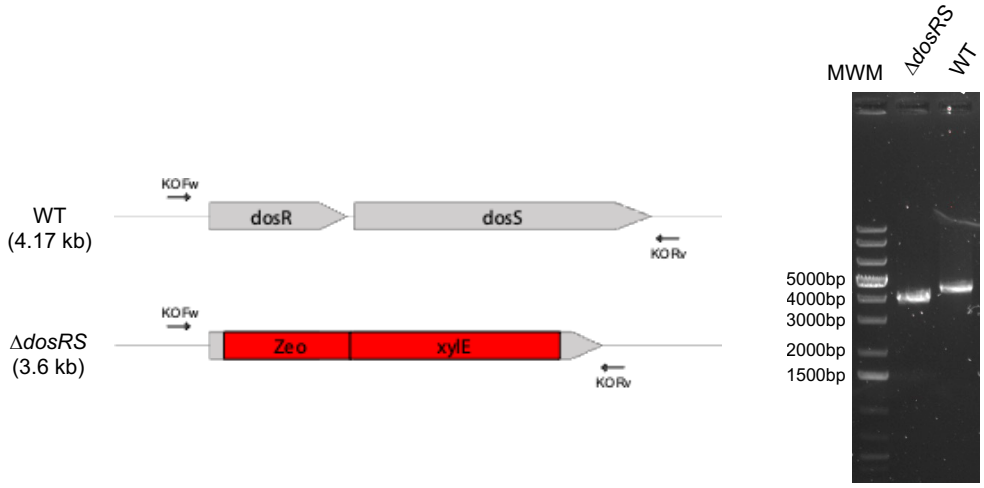

<u>Fig. S2</u>: Gene replacement at the *dosRS* locus of *Mabs* ATCC 19977.
Allelic replacement at the *dosRS* locus was confirmed by PCR using sets of primers (KOFw and KORv) located outside the linear allelic exchange substrate. The expected sizes of the products for the WT and mutant are indicated.

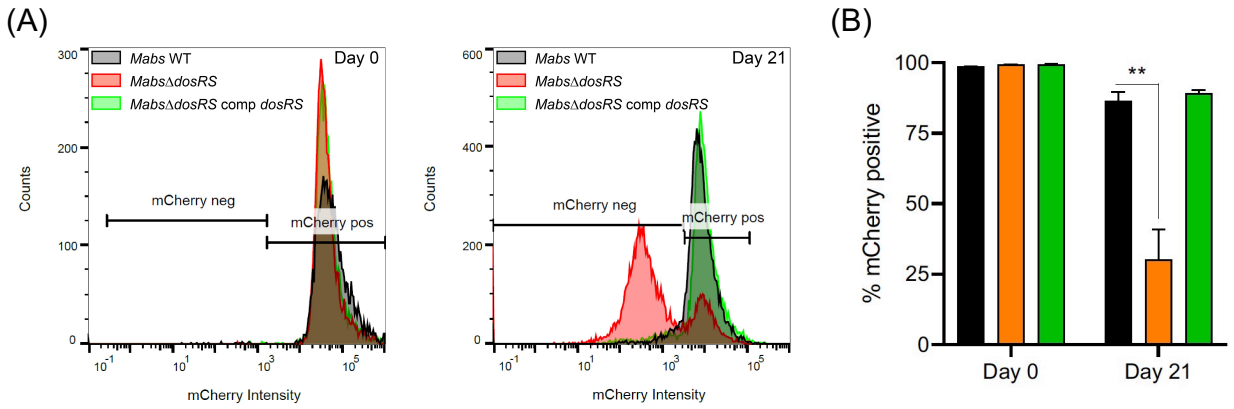

<u>Fig. S3</u>: Loss of viability of *MabsΔdosRS* in the Wayne model.
Flow cytometry analysis of mCherry-expressing WT *Mab*s ATCC 19977, *MabsΔdosRS* and *MabsΔdosRS* complemented with *dosRS* bacilli grown under hypoxic conditions in the Wayne model. (**A**) Representative histograms showing the proportion of mCherry-expressing (mCherry pos) and non-expressing (mCherry neg) bacilli for each strain on the day the cultures reached hypoxia (day 0; left panel) and after 21 days of incubation under hypoxic conditions (day 21, right panel). (**B**) Quantification of mCherry-positive bacilli on day 0 and day 21. The results show a clear decrease in the viability of *MabsΔdosRS* relative to the other strains after 21 days of hypoxic growth. The results presented are the means (± SD) of triplicate cultures. Asterisks denote statistically significant differences pursuant to the unpaired Student's *t*-test (**p<0.005).

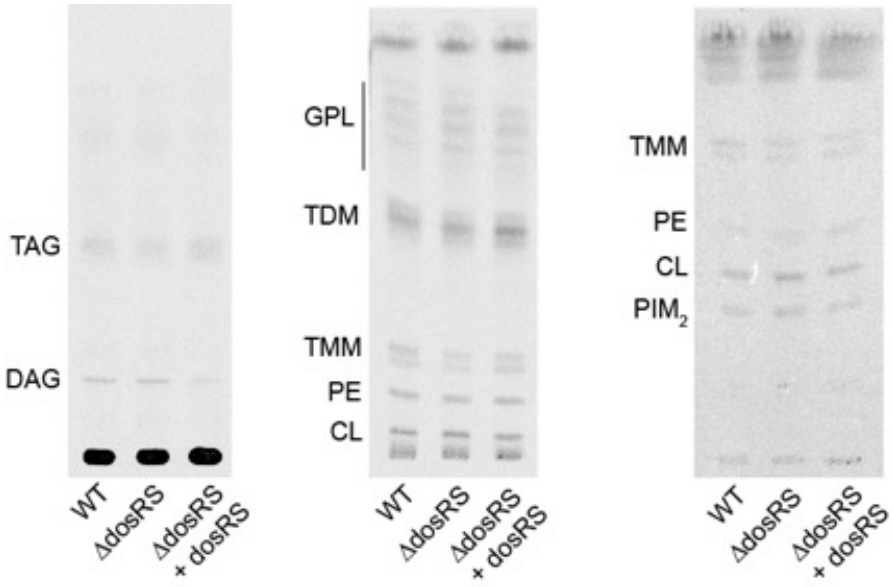

<u>Fig. S4</u>: Effect of knocking-out *dosRS* on *M. abscessus* lipid biosynthesis.
Mabs ATCC 19977 WT and *dosRS* KO were metabolically-labeled with [1,2-^{14}C]acetic acid for 24 hours in Dubos-Tween albumin broth under microaerophilic conditions in standing T25 vented flasks. Extracted total lipids from each strain (1,500 dpm per lane) were analyzed by TLC using different solvent systems to resolve lipids of different polarities (from left to right: [hexane:diethyl ether:acetic acid; 70:30:1 by vol.]; [chloroform:methanol:water; 20:4:0.5 by vol.]; [chloroform:methanol:water; 60:30:6 by vol.]). TAG (triacylglycerides); DAG, diacylglycerides; TDM, trehalose dimycolates; TMM, trehalose monomycolates; PE, phosphatidylethanolamine; CL, cardiolipin; PIM_2, phosphatidyl-*myo*-inositol dimannosides. The results shown are representative of two independent experiments.

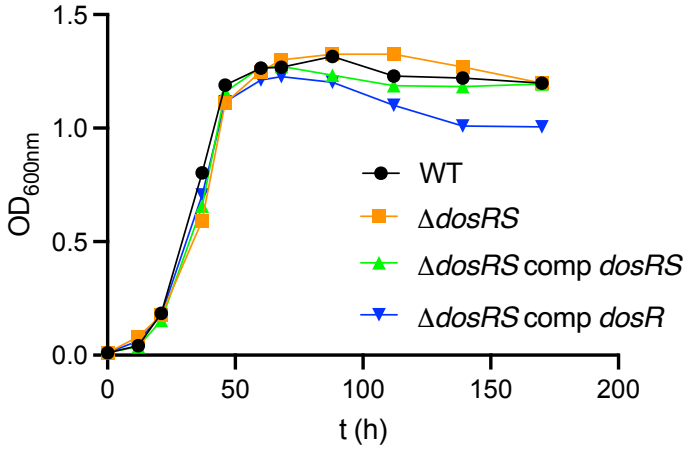

<u>Fig. S5</u>: Growth characteristics of *Mabs* ATCC 19977 WT, the *dosRS* KO and the *dosR* and *dosRS* complemented mutant strains in SCFM at 37°C.
The results shown are representative of two independent experiments.

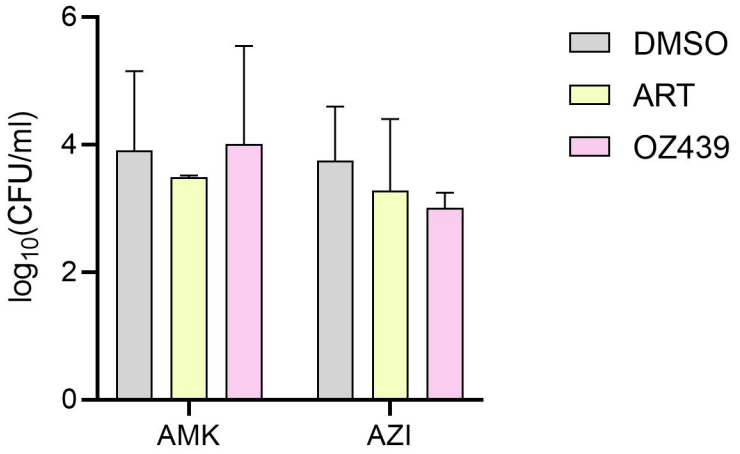

Fig. S6: Effect of DosS inhibitors on the drug tolerance of *Mabs*Δ*dosRS* under hypoxia.
The *Mabs dosRS* mutant was cultured in the Wayne model in the presence of DMSO, ART or OZ439 (40 μM each) from the time of inoculation. As cultures reached hypoxia, antibiotics [AMI (64 μg mL^{-1}) and AZI (32 μg mL^{-1})] and more DMSO or DosS inhibitors (40 μM each) were added and the cultures were incubated for another 7 days prior to CFU plating. As expected, DosS inhibitors had no significant effect (per the unpaired Student's *t*-test; $p < 0.05$) on the susceptibility of the *dosRS* mutant to AMI or AZI indicative of the on-target activity of ART and OZ439. The results presented are the means (± SD) of triplicate cultures.

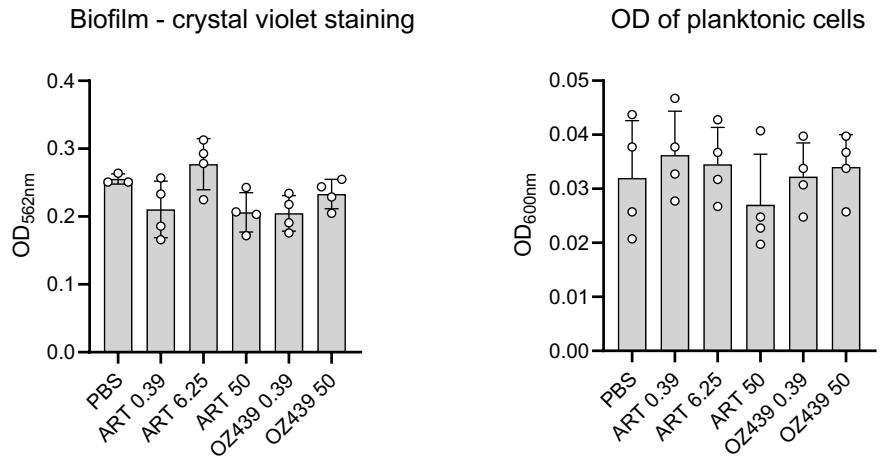

Fig. S7: Effect of DosS inhibitors on MABSC biofilm dispersal.
Four-day-old biofilms were washed with PBS and DosS inhibitors (or 0.05% DMSO as control) in PBS were added at the indicated concentrations (in μM). The plate was incubated for another 24 h at 37°C at which point biofilms were quantified by crystal violet staining and the turbidity of planktonic bacteria released in the medium assessed spectrophotometrically at 600 nm. The results presented are the means (± SD) of quadruplicate wells and are representative of two independent experiments.

<u>Fig. S8</u>: Identification of the *Mabs* DosR DNA-binding site.
Logo of the DosR-binding motif in *Mabs* ATCC 19977, based on 13 sites found in the promoter regions of DosR-regulated genes, including *MAB_0156c*, *MAB_1040*, *MAB_1041*, *MAB_1042c*, *MAB_2489*, *MAB_3134c*, *MAB_3354*, *MAB_3891c*, *MAB_3902c* and *MAB_3903* (see Table S1). The sequence was constructed using the WebLogo tool (*70*).

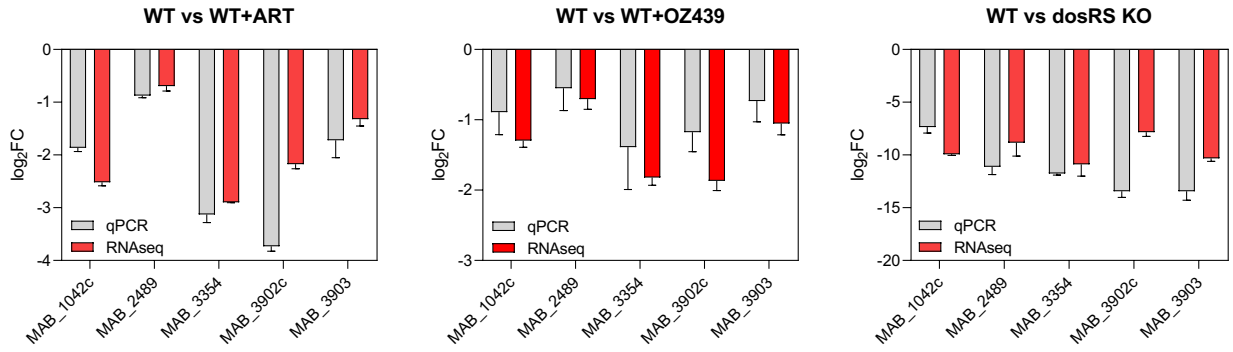

<u>Fig. S9</u>: Transcriptional profiles of ART- and OZ439-treated WT *Mabs* ATCC 19977 cells and of the *dosRS* KO mutant under microaerophilic growth conditions.
RNA-seq (log_2 fold-change) (red) and quantitative reverse transcription-PCR (RT-qPCR) (grey) show five genes expressed at lower level in the *dosRS* KO mutant or in ART- and OZ439-treated *Mabs* ATCC 19977 cells compared to untreated WT cells: *MAB_1042c* (*ctaD*, cytochrome c oxidase polypeptide I), *MAB_2489* (*usp*, universal stress protein), *MAB_3354* (*desA1*, desaturase), *MAB_3902c* (putative aminoglycoside phosphotransferase) and *MAB_3903* (putative Acg nitroreductase). All bacterial cultures were grown for 24 hours under microaerophilic conditions in standing T25 vented tissue culture flasks. Ratios of *genes*/*sigA* mRNA are means ± standard deviations (n = 3 RNA extractions and RT-qPCR reactions).

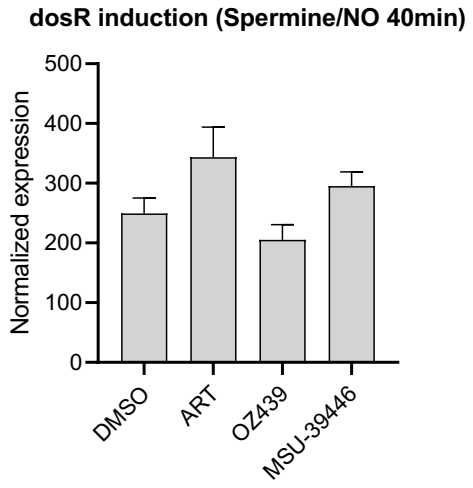

Fig. S10: Effect of DosS inhibitors on NO signaling.
Mabs ATCC 19977 was grown to OD ~ 0.3 in 7H9-ADC-Tween 80, treated for 1 h with either DMSO (control) or 50 μM of DosS inhibitors, followed by addition of Spermine NONOate (50 μM final concentration). Cells were further incubated with shaking for 40 min, collected and processed for quantitative reverse-transcription PCR of the *dosR* gene. *dosR* cDNA was normalized internally to the *sigA* cDNA in the same sample and *dosR* mRNA levels are expressed relative to the mRNA level of this gene in the absence of Spermine NONOate in the medium (arbitrarily set to 1). Ratios of *dosR*/*sigA* mRNA are means ± SD (n = 3 RNA extractions and RT-qPCR reactions).

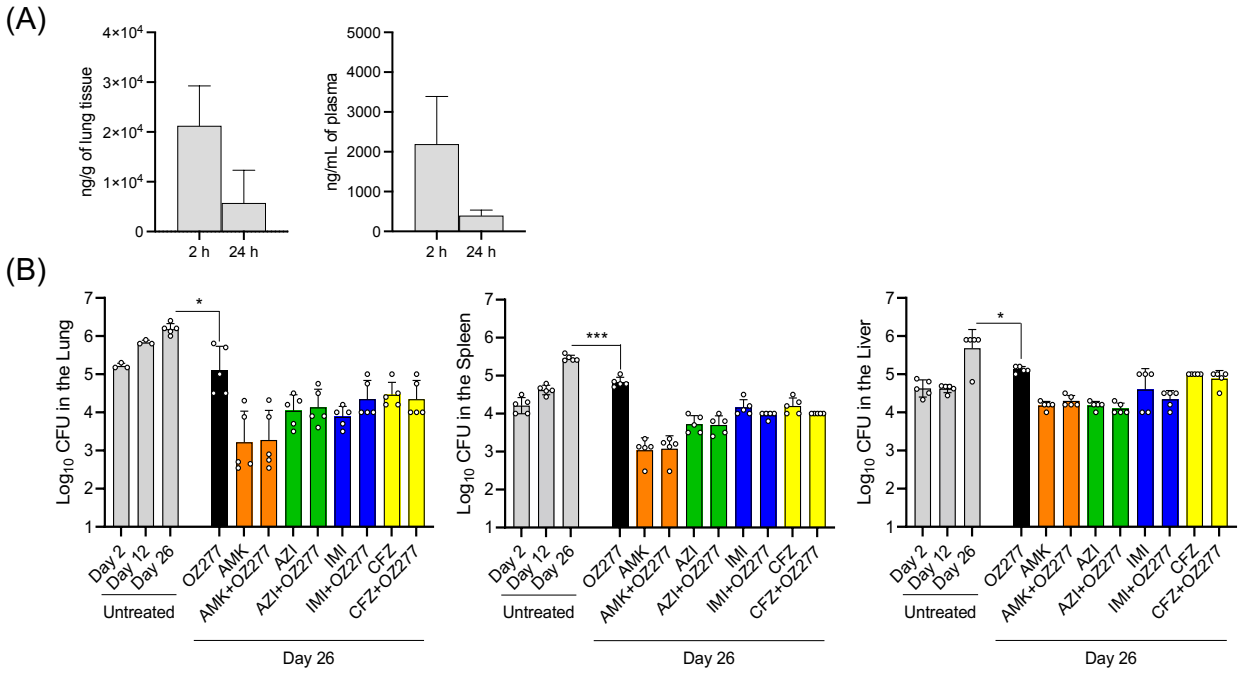

Fig. S11: Therapeutic efficacy of OZ277 in acutely MABSC-infected SCID mice.
(**A**) Exposure of OZ277 in *Mabs* ATCC 19977-infected SCID mice. Mice received OZ277 orally (200 mg/kg) daily for 14 days. Shown are the averages (± SD) of lung and plasma concentrations 2 and 24 hours after the last dosing. Two mice were used per time point.
(**B**) Therapeutic efficacy testing in an acute SCID mouse model of MABSC infection. Mice infected intratracheally with 10^6 CFUs of WT *Mabs* ATCC 19977 were treated daily as of day 12 for 14 days with HPMC-SV vehicle, OZ277 (200 mg/kg, gavage), AMK (150 mg/kg, subcutaneous injection), AZI (200 mg/kg, gavage), IMI (100 mg/kg, subcutaneous injection), CFZ (20 mg/kg, gavage), and the same four antibiotic treatments in combination with OZ277. Bacterial loads were determined in the lungs, liver and spleen on days 2, 12 and 26. Asterisks denote statistically significant differences between untreated and OZ277-treated mice (*$p < 0.05$; ***$p < 0.0005$). No statistically significant differences were noted between antibiotic-treated and antibiotic+OZ277-treated mice pursuant to the Student's *t*-test ($p < 0.05$).

Table S1: Characterization of the DosRS regulon of *Mabs* ATCC 19977.

List of differentially expressed genes between *Mabs* WT and *Mabs*Δ*dosRS* under microaerophilic conditions (log_2 FC<-2, *p*-value<0.05). Genes inhibited by ART and/or OZ439 and genes induced under NO stress are shown with their corresponding log_2 FC. Clusters of genes are colored. Asterisks denote genes that are likely to be part of operons with the first gene of the operon having a predicted DosR-binding site in its promoter region. [a]NO-induced genes are per ref. (*32*); [b]Predicted MABSC DosRS binding site. See Fig. S8; [c]Based on ref. (*28*).

Gene	Proposed function	WT vs *dosRS* KO	WT vs WT+ART	WT vs WT+ OZ439	Induction by NO[a]	MABSC DosR binding site[b]	*Mtb* ortholog	Belongs to *Mtb* DosRST regulon[c]
MAB_0156c	Iron-sulfur cluster-binding protein, RIESKE family	-2.05	-1.47			YES	Rv3818	
MAB_0714c	Hypothetical protein	-5.66						
MAB_0765	Hypothetical conserved integral membrane protein	-5.08	-2.81	-2.42				
MAB_0894c	Putative dihydrolipoamide dehydrogenase (LpdA)	-2.26					Rv0462c	
MAB_0911	Putative phenylacetate-CoA ligase	-2.23						
MAB_1040	Polyphosphate kinase 2 (PPK2)	-2.72	-1.93			YES	Rv3232c	
MAB_1041	Conserved hypothetical protein	-4.62	-2.47	-1.42	1.33	YES	Rv3129	YES
MAB_1042c	Probable cytochrome c oxidase polypeptide I ctaD	-9.95	-2.52			YES	Rv3043c	
MAB_1892	Hypothetical protein	-2.41						
MAB_2086c	Truncated transposase-like protein IS1601-D	-2.59						
MAB_2240	Putative ferredoxin	-2.76	-3.49					
MAB_2241	Putative nitrate ABC transporter, periplasmic protein	-2.82	-3.24					
MAB_2242	Putative nitrate ABC transporter, permease protein	-2.30	-3.17					
MAB_2243	Putative nitrate ABC transporter, ATP-binding protein	-2.05	-3.64					
MAB_2244	Fumarate reductase/succinate dehydrogenase flavoprotein-like FrdA	-2.06	-3.02					
MAB_2489	Universal stress protein	-8.85			6.26	YES	Rv2005c	YES
MAB_2490	Conserved hypothetical protein	-7.81			5.61	YES*	Rv2828c	
MAB_2509c	Conserved hypothetical protein	-2.74						
MAB_2512	Possible anti-anti-sigma factor	-2.01	-2.01			YES		
MAB_2530c	Catalase CatB	-2.37	-2.14					
MAB_2816c	Putative luciferase-like protein; putative oxidoreductase	-2.95						
MAB_3054c	Conserved hypothetical protein	-2.06						

MAB_3132c	Conserved transmembrane protein	-6.61			6.29	YES*	Rv2620c	
MAB_3133c	Putative flavohemoprotein	-8.01			7.33	YES*		
MAB_3134c	Transcriptional regulator, putative nitric-oxide sensor	-5.98			5.86	YES		
MAB_3354	Probable acyl-[acyl-carrier protein] desaturase DesA1	-10.89	-2.90	-1.82	3.70	YES	Rv0824c	
MAB_3355	Putative secreted SGNH-hydrolase	-2.18	-1.71	-1.48		YES*		
MAB_3433c	Conserved hypothetical protein	-2.04	-2.49					
MAB_3865	Conserved hypothetical protein	-2.00						
MAB_3902c	Aminoglycoside phosphotransferase family enzyme	-7.83	-2.18	-1.87	3.65	YES	Rv2004c	YES
MAB_3903	Putative nitroreductase, acg	-10.32	-1.32		6.11	YES	Rv2032	YES
MAB_3904	Universal stress protein	-7.70			5.17	YES*	Rv2028c	YES
MAB_3905	Hypothetical protein	-6.34				YES*		
MAB_3937	Hypothetical protein	-9.92	-1.58		6.78			
MAB_3938	Putative Clp protease subunit	-3.38	-1.74		2.38		Rv2667	
MAB_3962	Hypothetical cytochrome P450	-3.52						
MAB_4645	Conserved hypothetical protein	-2.01						
MAB_4839c	Putative transporter, MFS family	-2.24						

<u>Table S2</u> [see separate Excel file]: RNA-seq dataset of differentially expressed genes in all comparisons.

Differentially expressed (DE) genes in *Mabs* ATCC 19977 WT vs *Mabs*Δ*dosRS* or in any of these two strains either untreated or treated with ART or OZ439 were defined as ≥ 1 or ≤- 1 Log_2 fold changes in expression with a false discovery rate adjusted *p*-value < 0.05.

<u>Table S3</u> [see separate Excel file]: ssDNA oligo probes covering *Mabs* 16s and 23s rRNA used in rRNA depletion.